` **Load-Induced Modulation of Signal Transduction Networks**
Peng Jiang, Alejandra C. Ventura, Eduardo D. Sontag, Sofia D. Merajver, Alexander J. Ninfa and Domitilla Del Vecchio (11 October 2011)
Science Signaling **4** (194), ra67. [DOI: 10.1126/scisignal.2002152]

Science Signaling (ISSN 1937-9145) is published weekly, except the last week in December, by the American Association for the Advancement of Science, 1200 New York Avenue, NW, Washington, DC 20005.

COMPUTATIONAL BIOLOGY

Load-Induced Modulation of Signal Transduction Networks

Peng Jiang,[1] Alejandra C. Ventura,[2] Eduardo D. Sontag,[3] Sofia D. Merajver,[4] Alexander J. Ninfa,[1]* Domitilla Del Vecchio[5]*

Biological signal transduction networks are commonly viewed as circuits that pass along information—in the process amplifying signals, enhancing sensitivity, or performing other signal-processing tasks—to transcriptional and other components. Here, we report on a "reverse-causality" phenomenon, which we call load-induced modulation. Through a combination of analytical and experimental tools, we discovered that signaling was modulated, in a surprising way, by downstream targets that receive the signal and, in doing so, apply what in physics is called a load. Specifically, we found that non-intuitive changes in response dynamics occurred for a covalent modification cycle when load was present. Loading altered the response time of a system, depending on whether the activity of one of the enzymes was maximal and the other was operating at its minimal rate or whether both enzymes were operating at submaximal rates. These two conditions, which we call "limit regime" and "intermediate regime," were associated with increased or decreased response times, respectively. The bandwidth, the range of frequency in which the system can process information, decreased in the presence of load, suggesting that downstream targets participate in establishing a balance between noise-filtering capabilities and a circuit's ability to process high-frequency stimulation. Nodes in a signaling network are not independent relay devices, but rather are modulated by their downstream targets.

INTRODUCTION

A promising approach for unraveling the function of complex biological networks is to decompose them into functional modules (*1*, *2*) that have clearly defined functions, such as the sensing of extracellular ligands, signal transduction, gene expression, or control of metabolism. The goal is to characterize the emergent collective function of networks from knowledge of the behaviors of the individual modules, their interconnection topology, and the character of their interactions.

System dynamics, that is, the time-dependent behavior of the system, is critical in the process of delineating modules and determining their collective function as several researchers have remarked [see, for example, (*3*)]. At the genetic level, transcriptional networks encode various time-varying behaviors, such as the periodic changes of gene expression that are responsible for circadian rhythms and timing of the cell cycle (*4*, *5*). Metabolic reaction pathways are regulated by environmental stimuli that vary over time (*6*). The transient behavior of signaling systems controls gene activation patterns, as well as diverse physiological processes ranging from bacterial chemotaxis to cytoskeletal reorganization, to checkpoints in the cell cycle, and to apoptosis (*7*, *8*). Even when the steady-state amount of an activated signaling protein is within normal ranges, transient excess activation may result in aberrant signaling with severe consequences, such as cancer (*9*).

[1]Department of Biological Chemistry, University of Michigan Medical School, Ann Arbor, MI 48109–0606, USA. [2]Institute for Physiology, Molecular Biology, and Neuroscience, Department of Biology, and Laboratorio de Fisiología y Biología Molecular, Departamento de Fisiología, Biología Molecular y Celular, IFIBYNE-CONICET, Facultad de Ciencias Exactas y Naturales, Universidad de Buenos Aires, Ciudad Universitaria, Pabellón 2, Buenos Aires C1428EHA, Argentina. [3]Department of Mathematics, Rutgers University, New Brunswick, NJ 08854–8019, USA. [4]Department of Internal Medicine, Comprehensive Cancer Center, University of Michigan, Ann Arbor, MI 48109, USA. [5]Department of Mechanical Engineering, Massachusetts Institute of Technology, Cambridge, MA 02139, USA.
*To whom correspondence should be addressed. E-mail: aninfa@umich.edu (A.J.N.); ddv@mit.edu (D.D.V.)

We performed a study of system dynamics and modularity, specifically focusing on signal transduction circuits. A common view is that the operating characteristics of these circuits should not depend on the presence or absence of downstream targets, such as gene promoters or other proteins, to which they convey information. However, theoretical work (*10*–*13*) has suggested that the behavior of discrete modules might dramatically change in the presence of downstream targets through the effect of loads, just as in electrical, hydraulic, or mechanical systems. For covalent modification cycles, computational work has studied the effect of substrate sequestration on the cycle behavior (*14*–*16*). Specifically, it was shown that sequestration may account for dynamic effects such as signaling delay (*15*). In the context of gene regulatory networks, theoretical studies have shown that loading can decrease system bandwidth (*17*, *18*).

However, there has not been any experimental study of the dynamic effects of loads, nor have there been theoretical studies quantifying how the basic signal-processing time scales (response time and bandwidth) are affected. We used a combination of analytical and experimental tools and found that the time scales of signal communication were modulated by the concentrations of downstream targets ("loads") through a process that we term "load-induced modulation."

The present work complements studies of stoichiometric retroactivity (*19*), that is, the effect of sequestering by downstream targets on the steady states of an upstream system. Stoichiometric retroactivity is a phenomenon different from load-induced modulation, because stoichiometric retroactivity affects systems at steady state (*10*–*12*). By contrast, we demonstrate that even under conditions where the steady state of a component is unaffected by the presence of downstream targets (no stoichiometric retroactivity), the dynamic behavior of the system may be significantly altered by load-induced modulation (*10*–*12*). We provide mathematical and experimental evidence for the modulation of pathway dynamics by the presence of downstream targets.

As a model system, we chose a ubiquitous motif in signal transduction, the covalent modification cycle (Fig. 1A). Experimentally, we used the

reconstituted uridylyltransferase/uridylyl-removing enzyme (UTase/UR)–PII cycle, which is a model system derived from the nitrogen assimilation control network of *Escherichia coli* (*20*) (Fig. 1B). In this system of purified components, there are two enzymes (E_1, representing UTase, and E_2, representing UR) that are reciprocally controlled by an allosteric effector (u, representing Gln). E_1 and E_2 catalyze the interconversion of the unmodified (W, representing PII) and modified [W*, representing PII–UMP (uridine monophosphate)] forms of PII. PII is a homotrimer, and each subunit can be modified by uridylylation; modified subunits cannot bind to the downstream target protein NRII. However, because PII is a homotrimer, incompletely modified trimers can bind NRII through their unmodified subunits (Fig. 1B, right). We represent the effective load of NRII binding to any of the subunits of completely unmodified PII as λ (representing NRII that binds to unmodified trimers of PII) and the effective load resulting from NRII binding to an unmodified PII subunit from singly modified or doubly modified trimers of PII as α. Although in the experimental system studied here these loads are a protein (NRII), and the same protein interacts with both the modified and the unmodified forms of PII, loads can, in principle, be provided by any type of molecule that binds to either or both forms of the cycle substrate protein. The input of the system, u, is Gln, and the output of the system is the amount of the modified protein W* (PII-UMP). A variety of regulatory patterns are possible, and we consider in detail a model where u is an activator for E_2 and a noncompetitive inhibitor for E_1, because this pattern matches the UTase/UR–PII system (Fig. 1B). We considered the system "isolated" when there were no loads and "connected" when the load (NRII) was present. We also analyzed a mutated version of the UTase/UR–PII system in which the load (NRII) applied only to one side of the cycle (Fig. 1C). This mutated version of the cycle included a heterotrimeric form of the PII protein that behaved as if it was functionally monomeric.

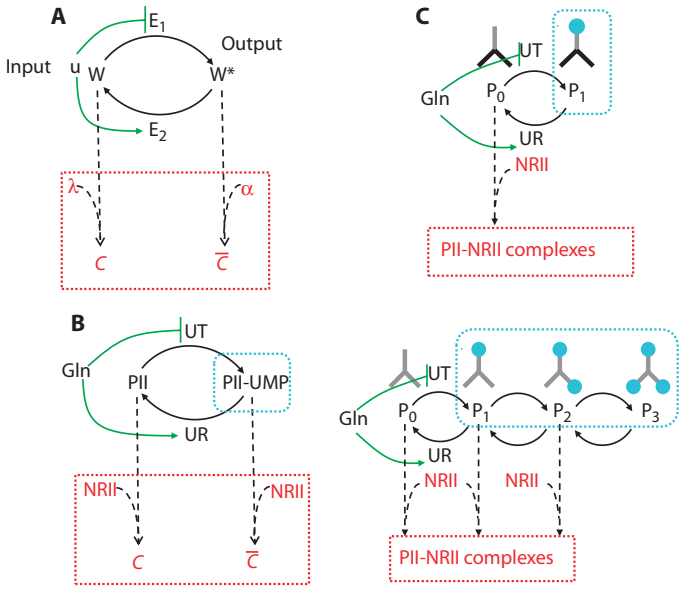

Fig. 1. The experimental system enables analysis of load-induced modulation of a signal transduction cascade. (**A**) General depiction of a covalent modification cycle. E_1 and E_2 represent the converter enzymes of the cycle, which are allosterically controlled by stimulatory effector u. The cycle protein W is interconverted to a modified form, W*. α and λ represent the effective load applied to W* and W, respectively, forming complexes $\overline{C}$ and C, respectively. That is, they represent the amount of downstream targets normalized by their dissociation constants (see Supplementary Materials, Model and Simulation, section 1). The input *u* is a periodic signal with frequency ω and amplitude A_0. (**B**) The UTase/UR–PII system. (Left) An abstracted view so that the correspondence with the modeled covalent modification cycle in (A) is evident. (Right) Detailed view of the double-load UTase/UR–PII cycle using wild-type PII trimers. The sequential modification of the three subunits of the PII trimer is depicted along with the complexes that are bound by NRII. Light blue circles signify the uridylyl groups that modify each subunit. Once modified by a uridylyl group, the modified subunit cannot bind NRII, although the remaining unmodified PII subunits of the trimer can bind NRII. PII-UMP represents the P_1, P_2, and P_3 species of PII because each of these has at least one modified subunit. Thus, the load NRII applies to both sides of the cycle. (**C**) Detailed view of the mutant UTase/UR–PII cycle used to represent a system with a single load. In most heterotrimeric PIIs, one of the three subunits is wild type, and two of the three subunits contain a mutation that prevents their interaction with NRII or UTase/UR. This "monovalent" P_1 PII heterotrimer is uridylylated and de-uridylylated in response to glutamine, but NRII binds only to the de-uridylylated P_0 PII; thus, the load applies to only one side of the cycle. Monovalent PII is depicted as containing two mutant subunits (black) and one wild-type subunit that can be reversibly modified or bind to NRII.

We analytically derived an extension of the standard Goldbeter-Koshland model for covalent modification (*21*) to include the effect of loads. On the basis of this mathematical model, we obtained analytical expressions for the response time and bandwidth as functions of the load and cycle parameters. We then used the frequency response, a control theory tool, to determine how time-varying signals were transmitted to measure the signaling system output in response to input signals that oscillated at different frequencies (*22*). By comparing the frequency response and the step response of the isolated system to those of the connected system, we determined how downstream loads affected system dynamics.

We found that the response to time-varying input stimuli was altered by the presence of loads, a phenomenon that we call load-induced modulation. When the level of the stimulus was either zero or at a high enough level to saturate the sensory capacity of the system, one of the cycle enzymes operates at its maximal rate, whereas the opposing activity operates at its minimal rate. We refer to this regime as the limit regime and found that the presence of the loads increased the response time (the time required for the system to transition between the "on" and the "off" states). By contrast, when the cycle enzymes operate in the presence of intermediate levels of stimulation, both enzymatic activities occur at intermediate rates. We refer to this regime as the intermediate regime and show that the presence of loads decreased the response time. The temporal profile of a stimulus determines how it is selectively transmitted through different cellular processes (*23*), and the quantity of information a pathway can carry depends on its bandwidth (*24*). We found that the presence of loads decreased system bandwidth and that the extent of the decrease depended on whether one or both of the modified and the unmodified forms of the substrate protein bound to a load. The effect of loads on bandwidth was more marked when only one of the two forms of the substrate protein was bound. Finally, when only one form of the substrate protein was bound by a downstream interacting target, the dynamical effects of the presence of the load were minimized by increasing the abundance of the cycle enzymes. Conversely, when both modified and unmodified forms of the substrate protein were bound by interacting targets, the dynamical effects of the presence of the loads were minimized by reduction in the abundance of the cycle enzymes.

RESULTS

Mathematical model description

We extended the standard ordinary differential equation (ODE) model for covalent modification by Goldbeter and Koshland (*21*) to include the effect of loads for either the unmodified or the modified substrate protein species (Supplementary Materials, Model and Simulation, section 1). For a species X, we represent the concentration of that species by X (italics). In the experimental system, we measured the amount of the total modified protein, that is, $\overline{W} := W^* + \overline{C}$, where $\overline{C}$ is the amount of the complex of the modified substrate protein bound to the load α (Fig. 1A). The ODE describing the dynamics of $\overline{W}$ is given by Eq. 1 (derived in the Supplementary Materials, Model and Simulation, section 1):

$$\frac{d\overline{W}}{dt} = \frac{V_1}{(1 + u/k_D')} \frac{W_T - \overline{W}}{K_1(1+\lambda) + (W_T - \overline{W})} - V_2 \left(\frac{u}{\overline{k_D'} + u}\right) \frac{\overline{W}}{K_2(1+\alpha) + \overline{W}} \quad (1)$$

in which K_1 and K_2 are the Michaelis-Menten constants for the forward and backward modification reactions, respectively; W_T is the total amount of protein; $V_1 = k_1 E_{1T}$ and $V_2 = k_2 E_{2T}$ are the maximal rates of the forward and backward reactions, respectively (k_1,k_2 being the catalytic rates and E_{1T},E_{2T} being the total enzymes amounts); λ and α are the effective loads applied to W and W^*, respectively; u is the concentration of the stimulatory effector; and k_D and k_D' are the dissociation constants of the stimulatory effector with enzymes E_1 and E_2, respectively. When u is zero or very large, the enzyme activities $(1 + u/k_D')$ and $V_2 \left(\frac{u}{\overline{k_D'} + u}\right)$ operate at their extreme values or limits. We refer to this operating regime as the "limit regime," and we call the situation in which their activities are not saturated the "intermediate regime." In the limit regime, the cycle output will reach its extreme values, corresponding to fully modified ($\overline{W} = W_T$) or fully unmodified ($\overline{W} = 0$). In the intermediate regime, the cycle output will not reach its maximum or minimum values. When α = 0, the load is applied to W only. From the ODE in Eq. 1, we observed that the presence of the load increased the apparent Michaelis-Menten constants.

Modeling results for load-induced modulation of rise and decay times

The rise and decay times quantify the time the cycle takes to switch steady state in response to a constant input stimulation. These times are relevant for signaling systems and also for transcriptional networks, in which the turning on and off of a signaling pathway or of a gene has direct consequences on physiology (*25*). The rise time is the time the output of the cycle $\overline{W}$ takes to rise from 10 to 90% of its overall response, and the decay time is the time $\overline{W}$ takes to decay from 90 to 10% of its overall response. (We obtained similar results if we considered the changes of the output between different percentages of the overall responses, such as 5 and 95% or 1 and 99% (see Supplementary Materials, Model and Simulation, section 1.3.1). We analyzed two cases: (i) when the cycle transitions between on ($\overline{W} = W_T$) and off ($\overline{W} = 0$) states in response to extreme inputs $u = 0$ and u sufficiently large, respectively, to saturate the enzymes' activities (limit regime); (ii) when the cycle transitions between intermediate states corresponding to values of the input that do not saturate the enzymes' activities (intermediate regime).

Calculations of the rise and decay times using our model (see Supplementary Materials, Model and Simulation, section 1.3.1) gave the following expressions for the decay and rise times of the connected system in the limit regime:

$$t_{decay} = \frac{1}{V_2}(K_2(1+\alpha)\ln(10/1.1) + 0.8W_T) \quad (2)$$

$$t_{rise} = \frac{1}{V_1}(K_1(1+\lambda)\ln(10/1.1) + 0.8W_T) \quad (3)$$

From these two equations, the decay and rise times increase linearly with the amount of load, and we can predict that the system with load on both W (λ > 0) and W* (α > 0) would display increased decay and rise times compared to the isolated system (α = λ = 0) (Fig. 2A). A system that had load applied only to W (λ > 0, but α = 0) would display an increased rise time but the same decay time as that of the isolated system.

When we set the input stimulation so the enzymes operate in the intermediate regime, the presence of loads is predicted to result in faster responses (Fig. 2B). Specifically, this is predicted to occur when the isolated system operates in the ultrasensitive regime (K_1,$K_2 \ll W_T$), where the response is switch-like, and the load is sufficient to make $K_1(1 + \lambda)$,$K_2(1 + \alpha) \gg W_T$, such that the dose response for the loaded system becomes more graded (Supplementary Materials, Model and Simulation, section 1.1; fig. S1). We could achieve this situation in our experimental system by using a concentration of PII that saturated the UTase and UR activities of the UTase/UR in the absence of NRII, but which was not saturating in the presence of NRII (*19*).

The presence of loads can have asymmetrical effects on the rise and decay times, causing one to increase while the other decreases. This is predicted to occur when, in addition to having K_1,$K_2 \ll W_T$ and $K_1(1 + \lambda)$,$K_2(1 + \alpha) \gg W_T$, the forward and reverse reactions of the covalent modification cycle have different Michaelis-Menten constants or catalytic rates (Fig. 2C). Both of these conditions can be obtained in our experimental system, because the UTase (E_1) and UR (E_2) activities of the UTase/UR have different Michaelis-Menten constants and catalytic rates.

Load-induced modulation of the bandwidth

The bandwidth of a system is the frequency band in which the system can process information. Here, we examined how the same cycle can display different bandwidths depending on the specific configuration and amounts of the loads. Let $A(\omega)$ be the amplitude of the output response to periodic input stimuli of period $T = 2\pi/\omega$. The bandwidth, denoted ω_B, is defined as the frequency at which the amplitude of the response $A(\omega)$ drops below the amplitude of the response to constant stimulation divided by the square root of 2 [$A_0/\sqrt{2}$]. A quantitative relationship between the bandwidth and the amounts of load can be determined by calculating the amplitude of response from the model under the assumption of small-amplitude sinusoidal input stimuli (about a mean value of u_0) of the form $u(t) = u_0 + A_0 \sin(\omega t)$ (see Supplementary Materials, Model and Simulation, section 1.4; figs. S2 and S3). Even though sinusoidal inputs may not be biologically relevant, the system response to these inputs provides general information on the amplitude of response and bandwidth for more complicated input profiles. To complement the analysis on the basis of sinusoidal inputs, we also considered input profiles in the form of a train of exponentially decaying pulses, which are biologically relevant and closer to the inputs in the experimental system, and obtained the same qualitative results (see Supplementary Materials, Model and Simulation, section 1.5; fig. S4).

For the connected system, the model states that the bandwidth expression is proportional to the total amounts of enzymes E_{1T} and E_{2T} and to

the catalytic rates k_1,k_2 and is inversely proportional to the concentrations of the loads λ and α when the isolated system steady-state response is hyperbolic (K_1,$K_2 \geq W_T$; see Supplementary Materials, Model and Simulation, section 1.4, for the exact bandwidth calculations). For large loads λ and α, the bandwidth of the connected system is predicted to be lower than that of the isolated system, that is, $\omega_B^C < \omega_B^I$, where "C" stands for "Connected" and "I" stands for "Isolated" (fig. S2). More generally, according to the model, the expressions of the bandwidths depend on the amounts of load, on the operating regime of the isolated system [ultrasensitive (K_1,$K_2 \ll W_T$) or hyperbolic (K_1,$K_2 \geq W_T$)], and on the input amplitude (whether it is such that the enzymes operate in the limit or intermediate regimes) (Fig. 3). Sufficiently high amounts of load decreased the bandwidth of the connected system compared to that of the isolated system (Fig. 3). However, for a fixed amount of load, the model predicted that decreasing the input amplitude (making the enzymes operate well within the intermediate regime) would decrease the difference between the isolated and the connected system bandwidths (Fig. 3A). If the input amplitude were set to sufficiently low values so the cycle enzyme operated well within the intermediate regime and the isolated system was operating in the ultrasensitive regime (K_1,$K_2 \ll W_T$), then small amounts of load can theoretically increase system bandwidth (Fig. 3, A and B). If the isolated system was operating in the hyperbolic regime (K_1,$K_2 \geq W_T$), then any amount of load would decrease system bandwidth independently

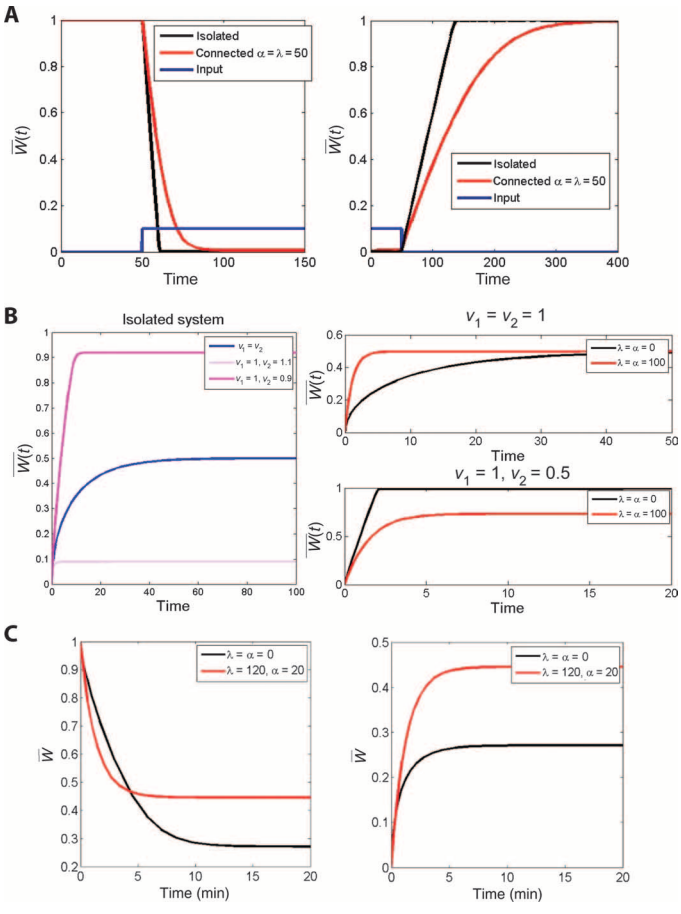

Fig. 2. Results of the model predictions for the effects of load-induced modulation on the rise and decay times of a covalent modification cycle. (**A**) The effect of load on the rise and decay of the reactions in the limit regime. In the simulation, the values of the parameters were set as V_1 = 0.012, V_2 = 0.12, $K_1 = K_2$ = 0.01, W_T = 1, $k_D = k_D'$ = 10, and α = λ = 50. In the left plots, the input suddenly changes at time 50 from u = 0 to u = 50, whereas in the right plot it changes from u = 50 to u = 0. The blue plot shows the input profile normalized by a factor of 500. Both the rise and the decay times increase due to the presence of the load. (**B**) Effect of load on the rise and decay of the reactions in the intermediate regime. (Left) Effect of the difference $v_1 - v_2$ on the isolated system rise time. When $v_1 - v_2 = 0$, the rise time is substantially larger than when $v_1 - v_2 \neq 0$. (Right) When $v_1 - v_2 = 0$, the rise time of the isolated system is substantially larger than the rise time of the connected system, whereas as the difference between v_1 and v_2 increases, the rise time of the connected system becomes larger than that of the isolated system. In these simulations, we have set $K_1 = K_2$ = 0.01 and W_T = 1. (**C**) The effect of load on the rise and decay of the reactions in the intermediate when $K_1 \neq K_2$. In the simulations, we have set K_1 = 0.01, K_2 = 0.06, λ = 120, α = 20, and v_1 = 0.83, v_2 = 1. Whereas the decay time is smaller for the connected system, the rise times of the connected and isolated systems are about the same.

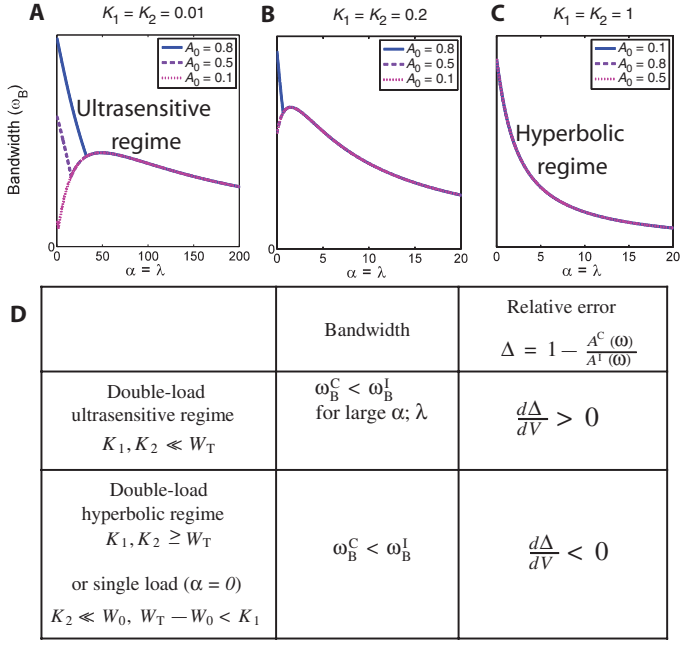

D

	Bandwidth	Relative error $\Delta = 1 - \frac{A^C(\omega)}{A^I(\omega)}$
Double-load ultrasensitive regime $K_1, K_2 \ll W_T$	$\omega_B^C < \omega_B^I$ for large α; λ	$\frac{d\Delta}{dV} > 0$
Double-load hyperbolic regime $K_1, K_2 \geq W_T$ or single load (α = 0) $K_2 \ll W_0$, $W_T - W_0 < K_1$	$\omega_B^C < \omega_B^I$	$\frac{d\Delta}{dV} < 0$

Fig. 3. Results of the model predictions for the effects of load-induced modulation on the bandwidth of a covalent modification cycle. Bandwidth is affected by load, the input amplitude, and the cycle operating regime. (**A** to **C**) (A) The effect of load on the bandwidth for different input amplitudes when the cycle operates in the ultrasensitive regime because K_1,$K_2 \ll W_T$. (B) The effect of load on the bandwidth for different input amplitudes when the cycle operates between ultrasensitive and hyperbolic regimes. (C) The effect of load on the bandwidth for different input amplitudes when the cycle operates in the hyperbolic regime because K_1,$K_2 \geq W_T$. For (A) to (C), $k_D = k_D'$ = 2, $V_2 = k_D' V_1$, and W_T = 1. The isolated system corresponds to the "0" point on the horizontal axis. (**D**) Table summarizing the effect of load-induced modulation on bandwidth. Here, ω_B denotes the bandwidth of the cycle, the superscripts denote "connected" (C) and "isolated" (I), and V is proportional to the amounts of enzymes.

of the input amplitude (Fig. 3C). Finally, in the system with single load, the decrease of bandwidth is more dramatic compared to the case in which $\lambda = \alpha > 0$ (see Supplementary Materials, Model and Simulation, section 1.4).

Insulation from loading by varying enzyme amounts

To understand whether a covalent modification cycle can operate under conditions that minimize the effects of loading and make the cycle effectively "insulated" from downstream targets, we examined the cycle behavior when the amounts of enzymes were changed. In particular, we examined the relative error $\Delta = \frac{A^I(\omega) - A^C(\omega)}{A^I(\omega)}$ between the amplitudes of the connected and the isolated system responses as a measure of the extent of the effect of loading (Fig. 3D and fig. S3; Supplementary Materials, Model and Simulation, section 1.4.1). The model predicted that the effect of changing the amounts of the enzymes depended on whether the isolated system operated in the ultrasensitive or hyperbolic regime. Specifically, the model predicted that when the isolated system operated in the ultrasensitive regime, decreasing the amounts of enzymes would make the amplitudes of the isolated and connected systems approach each other, reducing the relative error (Fig. 3D and fig. S3). When the isolated system operated in the hyperbolic regime, decreasing the amounts of enzymes would make the amplitudes of the isolated and the connected systems become far apart from each other, increasing the relative error (Fig. 3D; see Supplementary Materials, Model and Simulation, section 1.4.1). Finally, when the load was applied to one side only, for inputs operating at sufficiently low values (the input mean value u_0 is sufficiently small), decreasing the amounts of enzymes would make the amplitudes of the isolated and connected systems become farther apart from each other (see Supplementary Materials, Model and Simulation, section 1.4.1). These predictions and the results of the simulations are summarized in Fig. 3D, in which we have denoted $V = V_1$ and $V_2 = aV_1$, for some positive constant a, and W_0 is the equilibrium value corresponding to the input mean value u_0. In summary, the model predicted that if the isolated system operates in the ultrasensitive regime, an effective mechanism to attain dynamic insulation from loads would be to decrease the amount of the cycle enzymes; if the isolated system operates in hyperbolic regime or the load is applied to one side only, increasing the amounts of enzymes would be an effective mechanism to attain insulation.

Detailed description of the experimental model system

The reconstituted UTase/UR–PII covalent modification cycle of *E. coli* was used in the experiments (Fig. 1B) (*20*). The UTase/UR enzyme catalyzes the uridylylation of the PII protein through its UTase activity and catalyzes the de-uridylylation of PII-UMP through its UR activity. These reactions are regulated by glutamine (Gln), an allosteric effector that binds to a sensory domain on the UTase/UR to inhibit the UTase activity and activate the UR activity. Reactions are also regulated by α-ketoglutarate and adenylate energy charge, which are allosteric regulatory molecules that bind directly to PII and affect its ability to activate or inhibit its downstream targets (*26*, *27*). We performed the experiments at a fixed α-ketoglutarate concentration and at high adenosine triphosphate (ATP)/adenosine diphosphate (ADP) ratio so that the system responded to glutamine as its sole stimulatory effector, producing changes in PII uridylylation state in response to changes in glutamine (*25*). This system is analogous to covalent modification cycles involving phosphorylation and dephosphorylation. PII and PII-UMP interact with various downstream targets involved in nitrogen assimilation (*28*). Here, we studied the effect of one of the PII downstream targets, the NRII protein of *E. coli* (*20*), on the transient response of the UTase/UR–PII cycle to time-varying concentrations of glutamine. Use of a reconstituted system of purified proteins allowed us to examine conditions where NRII binding to PII provided a substantial load on the system and allowed us to vary the levels of the UTase/UR more than two orders of magnitude to identify conditions that mitigate load-induced modulation. Hence, our results are likely to be relevant for other signaling systems, where downstream targets are found at high concentrations and substantial loading effects are anticipated [for example, (*24*, *29*–*31*)].

The PII protein is a trimer; thus, its uridylylation state can vary from zero to three modifications per trimer (Fig. 1C). Hence, comparing the generalized model (Fig. 1A) with the details of the experimental model (Fig. 1B), W represents unmodified PII (P_0 of Fig. 1B), and the modified protein W* comprises all of the modified forms of PII (P_1, P_2, and P_3 of Fig. 1B). To study a circuit configuration where the load is applied to only one form of the protein (Fig. 1C), we used a mutated system (*19*) with a population of PII trimers, mostly heterotrimers, in which one of the three subunits is wild type and two of the three subunits contain a mutation that prevents their interaction with NRII or UTase/UR (Fig. 1C). This heterotrimeric form of PII, which we refer to as "monovalent PII," is uridylylated and de-uridylylated by the UTase/UR in response to glutamine on its wild-type subunit, but its two mutant subunits neither bind to NRII nor are able to become modified (*19*).

The effect of load-induced modulation on rise and decay times in the UTase/UR–PII system

We analyzed the behavior of the system when operating in the limit regime. To examine the rise time, we incubated the UTase/UR and PII with all necessary reaction components except uridine triphosphate (UTP) (which contained [α-^{32}P]UTP to allow measurement of uridylylation), and at time zero in the experiment, we added UTP. To examine the decay time, we incubated the intact system, including UTP, in the absence of glutamine for sufficient time to allow it to reach the steady state corresponding to almost complete uridylylation of PII, after which we added glutamine to the saturating concentration of 10 mM. We performed these experiments for both the isolated (without NRII) and the connected (with NRII) systems, for systems with wild-type PII and monovalent PII. Recall that the rise was defined as the time it takes for the output to rise from 10 to 90% of its overall response, and the decay time is the time it takes for the output to decay from 90 to 10% of its overall response.

As expected from Eqs. 2 and 3, NRII increased both the rise time (Fig. 4A) and the decay time (Fig. 4B) for the double-load system containing wild-type PII (corresponding to Fig. 1B). The presence of load altered only the initial response; the final steady state was not affected. When monovalent PII was used in the single-load system (corresponding to Fig. 1C), NRII increased the rise time (Fig. 4C) but did not affect the decay time (Fig. 4D), as expected from Eqs. 2 and 3, with $\alpha = 0$. With the amount of NRII used in our experiments, the decay time doubled (going from 6 min in the isolated system to 12.4 min in the connected system; Fig. 4A), and the rise time increased by a factor of 4.75 (going from 4 min in the isolated system to 19 min in the connected system; Fig. 4B) in the system containing wild-type PII. In the system containing monovalent PII, the rise time was increased by a factor larger than 4, going from 24 min in the isolated system to more than 70 min in the connected system (Fig. 4C).

To measure the decay time upon intermediate stimulation representing the system operating in the intermediate regime, we allowed isolated and connected systems with wild-type PII to evolve in the absence of glutamine until the steady state had been obtained (corresponding to high uridylylation), after which we added glutamine to intermediate values (0.5, 0.8, and 1.5 mM). At 0.8 mM glutamine, the connected system displayed a decreased response time relative to that of the isolated system, because the decay time of the isolated system was 10.6 min, whereas that of the connected system was 8 min (Fig. 4E). That is, the connected system reached its minimum faster than the isolated system. This is consistent

with our theoretical analysis showing that the presence of load made the response faster (Supplementary Materials, Model and Simulation, section 1.3.2). In the parallel experiments where glutamine was 0.5 mM, no significant difference between the decay times of isolated and connected systems could be discerned (fig. S5A), as expected (Supplementary Materials, Model and Simulation, section 1.3.2). When glutamine was 1.5 mM (fig. S5C), the connected system was also faster than the isolated system, but the difference appeared to be smaller than when glutamine was 0.8 mM (fig. S5B).

To measure the rise time upon intermediate stimulation, we included various concentrations of glutamine (0.5, 0.8, and 1.5 mM) in the reaction mixtures from the outset. Under these conditions, the steady-state uridylylation level corresponds to a lower concentration of uridylylated subunits than that obtained in the absence of glutamine. In contrast to the decay times, the rise times were slower in the connected system, and the difference between the connected and isolated systems became smaller as the glutamine concentration was increased (Table 1). We also examined the rise time of the system containing monovalent PII, in the presence of intermediate glutamine concentrations (0.4 and 0.6 mM); under both of these conditions, the difference between connected and isolated systems was larger than was the case in the absence of glutamine. Thus, in our experimental systems, the presence of load had asymmetrical effects at intermediate stimulation; it decreased the decay time but increased the rise time (Fig. 4E and Table 1).

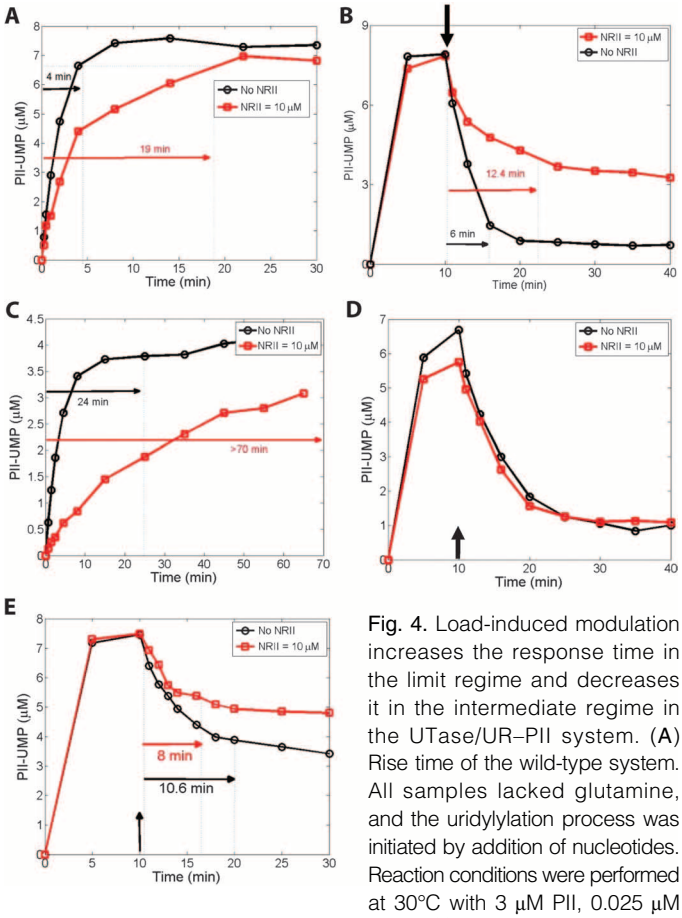

Fig. 4. Load-induced modulation increases the response time in the limit regime and decreases it in the intermediate regime in the UTase/UR–PII system. (**A**) Rise time of the wild-type system. All samples lacked glutamine, and the uridylylation process was initiated by addition of nucleotides. Reaction conditions were performed at 30°C with 3 μM PII, 0.025 μM UTase/UR, 0.2 mM α-ketoglutarate, 1 mM [α-^{32}P]UTP, 1 mM ATP, BSA (0.3 mg/ml), and ±10 μM NRII. PII-UMP was measured as previously described (*25*) (4 min and 19 min represent the rise times for the system without and with NRII, respectively). (**B**) Decay time for the wild-type system. After allowing the complete uridylylation of PII in the absence of glutamine, a saturating concentration of glutamine (10 mM) was added at 10 min (down-pointing arrow). Reaction conditions were as in (A), except that UTase/UR was 1.5 μM. The decay times for the system without and with NRII are 6 and 12.4 min, respectively. (**C**) Rise time of the system containing monovalent PII. Reaction conditions were as in (A) except that heterotrimeric PII formed from a 1:6 ratio of wild-type to PII–Δ47-53 subunits was used, at a concentration of 2 μM wild-type subunits, and UTase/UR was 0.012 μM. For the isolated system, the rise time was 24 min. The connected system failed to reach the steady state after more than 70 min. (**D**) Decay time of system containing monovalent PII. Reaction conditions were as in (C), except that UTase/UR was 0.5 μM and glutamine was added to 10 mM at 10 min (up-pointing arrow). (**E**) Decay time of system operating in the intermediate regime with wild-type PII and 0.8 mM glutamine (nonsaturating concentration) added at 10 min (up-pointing arrow). The decay times for the system with and without NRII are 8 and 10.6 min, respectively. In all panels, black represents the isolated system (without NRII), and red, the connected system (with NRII).

The effect of load-induced modulation on the bandwidth of the UTase/UR–PII system

Experimentally determining system bandwidth requires a method for imposing a time-varying input stimulation on the system. In our experimental system, the stimulatory effector is the amino acid glutamine. To remove glutamine from the system, we included a purified glutaminase [pyridoxal phosphate synthase (PLPS) from *Geobacillus stearothermophilus*]. Periodic injection of glutamine in the presence of the glutaminase resulted in a sharp rise in the glutamine concentration upon injection, followed by an exponential decay of the glutamine concentration, similar to the output that may result from a relaxation-type oscillator. We varied the rate of decay of glutamine and amplitude of the response to glutamine injection by altering the concentration of the glutaminase in the system, varied the amplitude of input stimulation simply by injecting more glutamine (Supplementary Materials, Experimental Systems, section 2; fig. S6), and controlled the frequency of stimulation by injecting glutamine at the desired intervals.

The response of the reconstituted UTase/UR–PII system to periodic changes in glutamine concentration in the presence or absence of NRII showed that the presence of load affected both the amplitude and the bandwidth of the wild-type (Fig. 5, A and B) and the monovalent PII (Fig. 5, C and D) systems. Amplitudes were estimated as described in the Supplementary Materials, Experimental Systems, section 2. In both

Table 1. Rise times for isolated (–NRII) and connected (+NRII) systems.

[Glutamine]	[UTase/UR] (μM)	Response time (–NRII) (min)	Response time (+NRII) (min)
Experiments with wild-type PII			
0 nM	0.025	4	15
0.3 mM	0.025	20	42
0.6 mM	0.025	61	70
0.9 mM	0.025	72	78
1.5 mM	0.025	72	80
Experiments with heterotrimeric PII			
0 nM	0.012	12	50
0.4 mM	0.025	40	72
0.6 mM	0.025	68	80

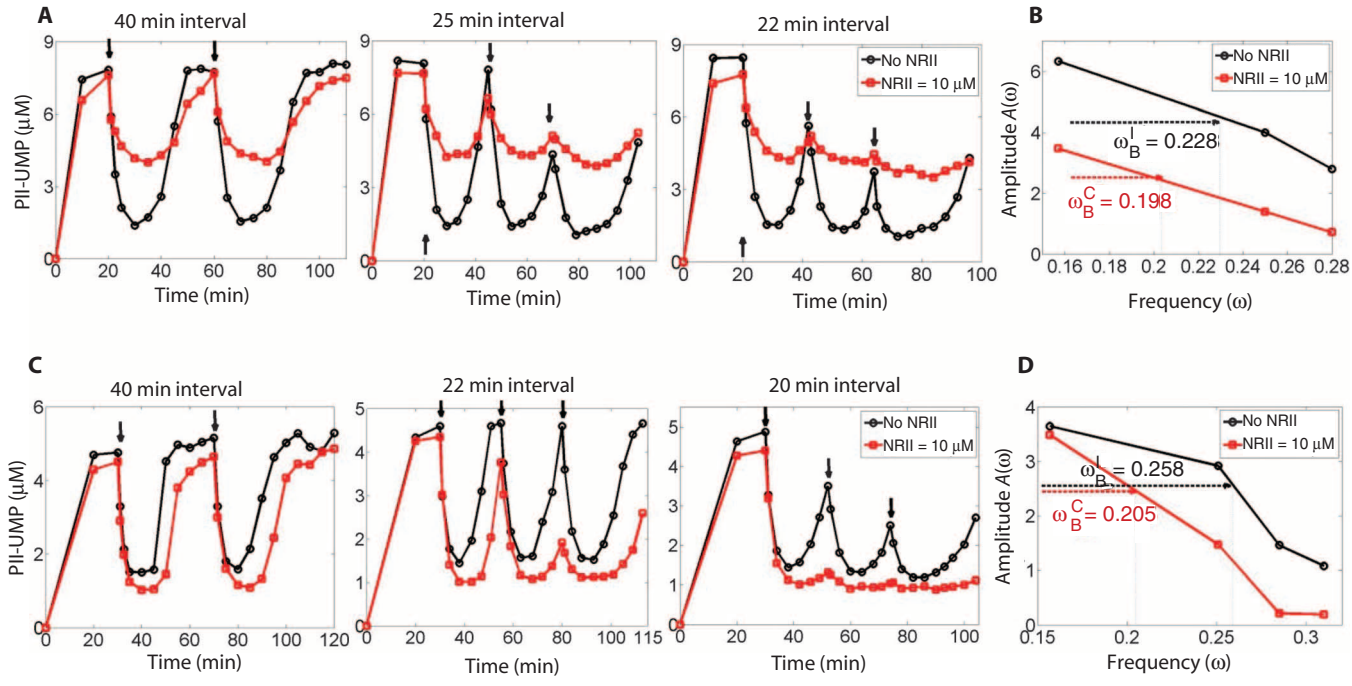

Fig. 5. Load-induced modulation decreases system bandwidth in the UTase/UR–PII system. (**A**) Performance of the UTase/UR–PII monocycle with periodic input stimulation of increasing frequency. The reaction mixtures contained 3 μM PII, 1.5 μM UTase, glutaminase consisting of 75 μM PLPS (24-mer) and additional 15 μM PdxT (to ensure saturation of PLPS with the T subunits), and 10 μM NRII (red curves and points □), or with no NRII (black curves and points ○). At indicated times (shown by the arrows), glutamine was added to 5 mM. For the left graph, glutamine was added at 20 and 60 min; for the middle graph, at 20, 45, and 70 min; and for the right graph, at 20, 42, and 64 min. (**B**) Replot of the amplitude as a function of the frequency ω of the input stimulation from the graphs in (A). The bandwidths for the isolated system ω_B^I and for the connected system ω_B^C are indicated by the arrows. For every frequency, the amplitude was calculated by taking the average of the excursions from each trough to each peak, starting from the first trough. (**C**) UTase/UR–PII system with monovalent PII as the substrate. The monovalent PII was formed from a 6:1 ratio of mutant to wild-type subunits and was used at a concentration of 2 μM wild-type subunits. The reaction conditions were the same as in (A), except UTase was 1 μM. For the left graph, glutamine was added at 30 and 70 min; for the middle graph, at 30, 52, and 74 min; and for the right graph, at 30, 50, and 70 min. (**D**) Replot of the amplitudes as a function of the frequency of the input from the graphs in (C).

cases, the presence of NRII caused a decrease in the amplitude of the response and in the bandwidth (Fig. 5, B and D). With wild-type PII, the presence of load caused a 13.2% decrease in bandwidth (Fig. 5B). In the single-load system with monovalent PII, load caused a 21% decrease of bandwidth. Also, for the single load, the amplitudes of responses at low frequency are the same for the isolated and connected system, and they diverge only at higher frequencies (Fig. 5D). The amplitude of response at low frequency was similar for the isolated and connected systems, but as the frequency of stimulation increased, the connected system amplitude dropped much faster than that of the isolated system (Fig. 5D). For both systems (with wild-type and monovalent PII), we identified an input frequency where the isolated system demonstrated a substantial response, whereas the connected system essentially failed to respond (Fig. 5, A, right, and C, right). Thus, the presence of load decreased the bandwidth of the covalent modification cycle and the amplitude of response.

Some characteristics of the experimental system also affected the profile of the response to changes in stimulation frequency. When the frequency of the input stimulation (addition of glutamine) increased, the peaks of the response tended to monotonically decrease. This is likely due in part to the transient response of the system, which was not yet extinguished in the duration of the experiment. (Simply stated, by the time the second injection of glutamine was applied, the system was still responding to the first injection.) This effect is due to the lag between changes in the glutamine concentration and changes in the PII modification state being sufficiently large, such that the PII modification state never reached its steady state before the next addition of glutamine. Also, when the input frequency was at the highest tested (Fig. 5, A, right, and C, right), it is likely that glutamine was not completely removed by the glutaminase and accumulated so that eventually the trajectories saturated to their low values. Finally, slow decay in the rate of the glutaminase activity during the course of the experiments seems to have occurred, because we observed a slight widening of each peak as the experiments progressed.

Theory predicted that for a fixed amount of load, decreasing input amplitude would decrease the difference between the isolated and the connected system bandwidths (Fig. 3, A and B). To study this, we performed experiments where a lower (nonsaturating) amount of glutamine was added with each injection. Figure 6 shows the responses to inputs at different injection frequencies, where each injection raised the glutamine concentration by 1.5 mM (as opposed to each injection raising the glutamine concentration by 5 mM, as in Fig. 5). Glutamine at 1.5 mM is well within the range that the system can sense (*32*), and a low concentration of glutaminase was used in the experiments, such that the rate of decay of glutamine was reduced compared to the experiments of Fig. 5. Unlike the experimental results obtained when a saturating concentration of glutamine was the

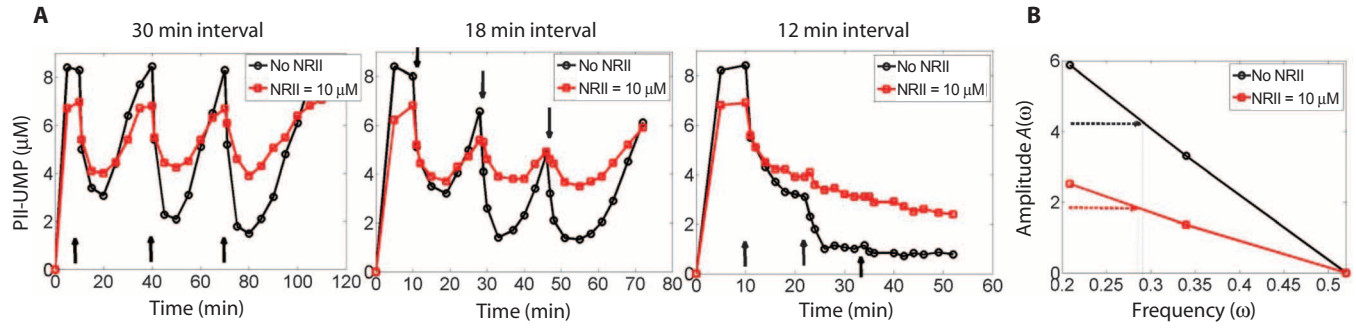

Fig. 6. Isolated and connected systems exhibit the same bandwidth under conditions of low-amplitude stimulation. (**A**) The UTase/UR–PII wild-type monocycle response to periodic input stimulation with increasing frequency for the isolated (black curves and points ○) and connected (red curves and points □) system with 10 μM NRII. The reaction conditions were the same as in Fig. 5A, except that pyridoxal phosphate synthetase was 50 μM, and glutamine was added to 1.5 mM at the indicated time points (as shown by the arrows). For the left graph, glutamine was added at 10, 40, and 70 min; for the middle graph, glutamine was added at 10, 28, and 46 min; and for the right graph, glutamine was added at 10, 22, and 34 min. (**B**) Replot of amplitude as a function of the frequency of the input from the graphs in (A).

input, none of the frequencies tested with this lower concentration of glutamine as the input resulted in a condition in which the isolated system responded and the connected system did not (compare Fig. 5C, right, where the injections were every 22 min, with Fig. 6, middle, where the injections were every 18 min). The bandwidths of the isolated and connected systems were similar (Fig. 6B), confirming the theoretical predictions. In our experiments, there is a limit to the frequency at which one can add glutamine, which is related to the concentration of glutamine added and the decay rate (glutaminase level). When the decay rate is very slow and the frequency of addition is high, glutamine will not be completely degraded after each pulse and will build up in the system. The accumulation of glutamine will result in lower amounts of PII uridylylation, as appeared to have occurred at the highest frequency of 1.5 mM glutamine addition (Fig. 6, right).

Insulation from load-induced modulation by varying the amounts of the cycle enzymes

The UTase/UR enzyme has both uridyltransferase- and uridylyl-removing activities, so the activities of both cycle enzymes can be simultaneously altered by performing experiments with different concentrations of UTase/UR. We performed experiments with the double-load system containing wild-type PII and the single-load system containing monovalent PII similar to those presented in Fig. 5, except with different amounts of UTase/UR. In the system with wild-type PII, decreasing the enzyme amounts decreased the difference between the output amplitudes of the isolated and connected systems (Fig. 7, A and B). The opposite pattern was observed when the system with monovalent PII was examined; increasing the amounts of enzyme made the amplitudes of the connected and isolated systems closer to each other (Fig. 7, C and D). The plots of the amplitudes as a function of the enzyme amounts (Fig. 7, B and D) include data from Fig. 5 with the same stimulation frequency at high enzyme concentration. This opposite effect of cycle enzyme concentration on the amplitudes of double load or single load connected compared to the amplitudes of the isolated systems is consistent with our theoretical predictions (Fig. 3D).

DISCUSSION

We illustrated through theory and experiments how the presence of load affects the dynamics of a covalent modification cycle, a common component of signaling networks. Specifically, we found that load-induced modulation controls the defining characteristics of dynamic behavior, response time, and bandwidth, in non-intuitive ways. Our methodology is based on comparing the step and frequency responses of a signaling component in an isolated system lacking any load to the same responses when the signaling component is connected to its downstream targets that function as load, which allowed us to capture the interaction between individual network modules and determine the emergent network behavior. We used as the experimental system a reconstituted covalent modification cycle of *E. coli*, which was used under conditions (amounts of substrate proteins, enzymes, and load targets) that are relevant for native signaling cascades. Hence, the effects that we report are expected to be observed in many signaling systems in vivo.

The frequency response determines a system's ability to respond to physiologically relevant signals with high amplitude and low frequency, while filtering out high-frequency, low-amplitude input signals that are not physiologically relevant (noise) (*33*). We found that the presence of downstream targets reduced the bandwidth of the system, thus altering the system's responsiveness by making it more limited than it would be in the absence of targets (Fig. 5). One potential application of this phenomenon that load-induced modulation can quench responses to time-varying stimulation is the development of small molecules as therapeutic loads that diminish aberrant signaling occurring in various disease states (*9*).

Evolution or human engineering of complex signaling networks may be facilitated by conditions that minimize load-induced modulation, because this would ensure modular behavior of the network. We showed that the amounts of the converting enzymes in a signaling system control the extent of the dynamic effects of load molecules and that dynamic insulation from these loads may be obtained by changing the amounts of cycle enzymes. This finding suggests a possible mechanism for attaining insulation from load molecules and hence for engineering insulation devices in synthetic biology (*10*, *34*). Of course, when engineering signaling systems, the presence of explicit negative feedbacks in signaling networks enhances robustness to downstream perturbations and hence also enables unidirectional signal propagation (*13*).

Load-induced modulation may be beneficial, providing an additional mechanism to tune the dynamic behavior of a system. For example, tuning the bandwidth of a system may be advantageous for increasing robustness to noise or for reducing crosstalk between pathways sharing common components (*35*).

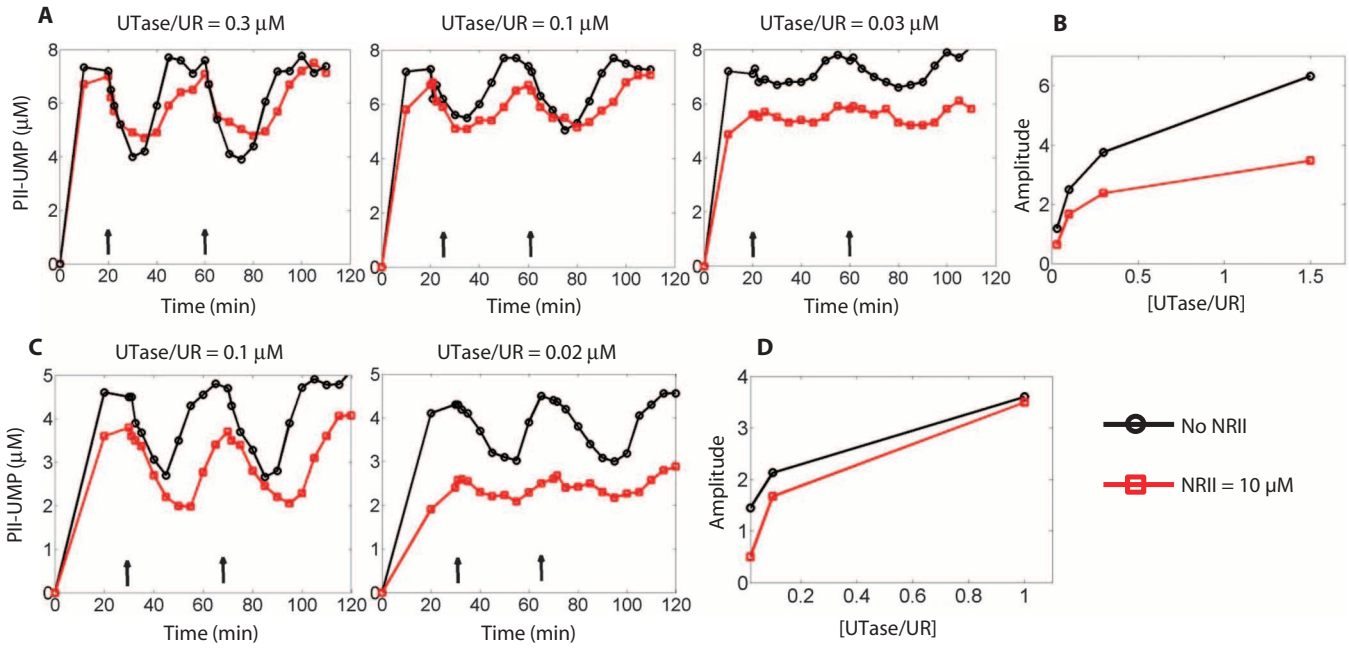

Fig. 7. Changing the enzyme amount affects the effect of load on the UTase/UR–PII system. (**A**) The double-load UTase/UR–PII wild-type system under periodic input stimulation with decreasing UTase amounts, with 10 μM NRII (□ red points and curves) or with no NRII (○ black points and curves). The reaction conditions were the same as in Fig. 5A, except that the UTase amount was varied. For the left graph, UTase was 0.3 μM; for the middle graph, UTase was 0.1 μM; and for the right graph, UTase was 0.03 μM. (**B**) Replot of amplitude as a function of UTase amounts from the graphs in (A) and from Fig. 5A (left). (**C**) The single-load UTase/UR–PII system with monovalent PII. The reaction conditions were the same as that of Fig. 5C, except that the UTase amount was varied. For the left graph, UTase was 0.1 μM, and for the right graph, UTase was 0.02 μM. (**D**) Replot of amplitude as a function of UTase amounts from graphs in (C) and from Fig. 5C (left).

Our study provided a mathematical and experimental basis for understanding how signaling modules and downstream targets are linked, due to load-induced modulation of signaling dynamics. This load-induced modulation of signaling properties has direct repercussions on emergent network behavior and, ultimately, on physiology.

MATERIALS AND METHODS

Model and simulation

Details of the model and derivations are described in the Supplementary Materials, Model and Simulation. Simulations were performed with MATLAB 7.11 and Simulink. Models are available as Simulink files.

Purified proteins

PII, UTase/UR, and NRII were prepared as described (*25*). Heterotrimeric monovalent PII was prepared as described (*19*). Briefly, we formed heterotrimeric PII by gently dissociating the subunits of wild-type and Δ47-53 mutant PII trimers, mixing at a ratio of six mutant subunits per wild-type subunit, and then allowing the subunits to reassociate. Under these conditions, most wild-type subunits become incorporated into trimers with two mutant subunits. For a glutaminase enzyme, we used PLPS from the thermophile *G. stearothermophilus*, which was purified as described (*36*). This glutaminase has a low K_m of ~0.5 mM glutamine, can be produced at high concentration, has suitable activity, and apparently does not interfere with our reconstituted systems.

UTase/UR–PII monocycle dynamic experiments

The reaction mixture contained 100 mM tris-Cl (pH 7.5), 10 mM $MgCl_2$, 100 mM KCl, bovine serum albumin (BSA; 0.3 mg/ml), 0.2 mM α-ketoglutarate, 1 mM ATP, 2 mM [α-^{32}P]UTP or as indicated, 3 μM PII (homotrimers), UTase/UR as indicated, NRII as indicated, and PLPS (24-meric complex, concentration stated as the concentration of each of the two types of subunits) as indicated. The reactions were performed at 30°C and were initiated by addition of a mixture of the nucleotides (UTP and ATP). After incubation for 10 to 30 min, glutamine was added to 5 mM (or as indicated). Aliquots were taken at time intervals and spotted onto P81 cellulose-phosphate filters (Whatman) and washed extensively in 5% trichloroacetic acid. The incorporation of radioactive label into PII was quantified by liquid scintillation counting. For dynamic experiments with monovalent PII, the reaction conditions and procedure were the same except wild-type PII was substituted by 2 μM heterotrimeric PII mixture, which was formed from a sixfold excess of Δ47-53 subunits over wild-type subunits (*25*). Figure S7 shows experiments testing the effect of applying the first injection of glutamine before the system had reached its steady state.

SUPPLEMENTARY MATERIALS

www.sciencesignaling.org/cgi/content/full/4/194/ra67/DC1

Text

Fig. S1. Steady-state effects of loading.

Fig. S2. Effect of loading on the frequency response.

Fig. S3. Effects of enzyme amounts.

Fig. S4. Effect of the load on the amplitude of response to a train of pulses.

Fig. S5. Response of the UTase/UR–PII cycle to stimulation with nonsaturating concentrations of glutamine.
Fig. S6. Using glutaminase and injections of glutamine to impose time-varying input stimulation.
Fig. S7. Amplitude of the initial response to glutamine addition depends on whether or not the system has achieved a steady state before glutamine addition.
References
SimulinkModel (.mdl file)

REFERENCES AND NOTES

1. U. Alon, Biological networks: The tinkerer as an engineer. *Science* **301**, 1866–1867 (2003).
2. L. H. Hartwell, J. J. Hopfield, S. Leibler, A. W. Murray, From molecular to modular cell biology. *Nature* **402**, C47–C52 (1999).
3. R. P. Alexander, P. M. Kim, T. Emonet, M. B. Gerstein, Understanding modularity in molecular networks requires dynamics. *Sci. Signal.* **2**, 1–4 (2009).
4. J. C. Dunlap, Molecular bases for circadian clocks. *Cell* **96**, 271–290 (1999).
5. M. T. Laub, H. H. McAdams, T. Feldblyum, C. M. Fraser, L. Shapiro, Global analysis of the genetic network controlling a bacterial cell cycle. *Science* **290**, 2144–2148 (2000).
6. T. Nishikawa, N. Gulbahce, A. E. Motter, Spontaneous reaction silencing in metabolic optimization. *PloS Comput. Biol.* **4**, e1000236 (2008).
7. C. J. Marshall, Specificity of receptor tyrosine kinase signaling: Transient versus sustained extracellular signal-regulated kinase activation. *Cell* **80**, 179–185 (1995).
8. A. Hoffmann, A. Levchenko, M. L. Scott, D. Baltimore, The IκB–NF-κB signaling module: Temporal control and selective gene activation. *Science* **298**, 1241–1245 (2002).
9. P. Blume-Jensen, T. Hunter, Oncogenic kinase signalling. *Nature* **411**, 355–365 (2001).
10. D. Del Vecchio, A. J. Ninfa, E. D. Sontag, Modular cell biology: Retroactivity and insulation. *Mol. Syst. Biol.* **4**, 161 (2008).
11. A. C. Ventura, J.-A. Sepulchre, S. D. Merajver, A hidden feedback in signaling cascades is revealed. *PLoS Comput. Biol.* **4**, e1000041 (2008).
12. J. Saez-Rodriguez, A. Kremling, E. D. Gilles, Dissecting the puzzle of life: Modularization of signal transduction networks. *Comput. Chem. Eng.* **29**, 619–629 (2005).
13. H. M. Sauro, B. N. Kholodenko, Quantitative analysis of signaling networks. *Prog. Biophys. Mol. Biol.* **86**, 5–43 (2004).
14. N. I. Markevich, J. B. Hoek, B. N. Kholodenko, Signaling switches and bistability arising from multisite phosphorylation in protein kinase cascades. *J. Cell Biol.* **164**, 353–359 (2004).
15. N. Blüthgen, F. J. Bruggeman, S. Legewie, H. Herzel, H. V. Westerhoff, B. N. Kholodenko, Effects of sequestration on signal transduction cascades. *FEBS J.* **273**, 895–906 (2006).
16. F. Ortega, L. Acerenza, H. V. Westerhoff, F. Mas, M. Cascante, Product dependence and bifunctionality compromise the ultrasensitivity of signal transduction cascades. *Proc. Natl. Acad. Sci. U.S.A.* **99**, 1170–1175 (2002).
17. S. Jayanthi, D. Del Vecchio, On the compromise between retroactivity attenuation and noise amplification in gene regulatory networks. *Proc. IEEE Conf. on Decision and Control* 4565–4571 (2009).
18. K. H. Kim, H. M. Sauro, Fan-out in gene regulatory networks. *J. Biol. Eng.* **4**, 16 (2010).
19. A. C. Ventura, P. Jiang, L. Van Wassenhove, D. Del Vecchio, S. D. Merajver, A. J. Ninfa, Signaling properties of a covalent modification cycle are altered by a downstream target. *Proc. Natl. Acad. Sci. U.S.A.* **107**, 10032–10037 (2010).
20. A. J. Ninfa, P. Jiang, M. R. Atkinson, J. A. Peliska, Integration of antagonistic signal in the regulation of nitrogen assimilation in *Escherichia coli*. *Curr. Top. Cell. Regul.* **36**, 31–75 (2000).
21. A. Goldbeter, D. E. Koshland Jr., An amplified sensitivity arising from covalent modification in biological systems. *Proc. Natl. Acad. Sci. U.S.A.* **78**, 6840–6844 (1981).
22. J. T. Mettetal, D. Muzzey, C. Gómez-Uribe, A. van Oudenaarden, The frequency dependence of osmo-adaptation in *Saccharomyces cerevisiae*. *Science* **319**, 482–484 (2008).
23. M. Behar, H. G. Dohlman, T. C. Elston, Kinetic insulation as an effective mechanism for achieving pathway specificity in intracellular signaling networks. *Proc. Natl. Acad. Sci. U.S.A.* **104**, 16146–16151 (2007).
24. P. Hersen, M. N. McClean, L. Mahadevan, S. Ramanathan, Signal processing by the HOG MAP kinase pathway. *Proc. Natl. Acad. Sci. U.S.A.* **105**, 7165–7170 (2008).
25. B. N. Kholodenko, J. F. Hancock, W. Kolch, Signalling ballet in space and time. *Nat. Rev. Mol. Cell Biol.* **11**, 414–426 (2010).
26. P. Jiang, A. J. Ninfa, Sensation and signaling of α-ketoglutarate and adenylylate energy charge by the *Escherichia coli* PII signal transduction protein require cooperation of the three ligand-binding sites within the PII trimer. *Biochemistry* **48**, 11522–11531 (2009).
27. P. Jiang, A. J. Ninfa, *Escherichia coli* PII signal transduction protein controlling nitrogen assimilation acts as a sensor of adenylylate energy charge in vitro. *Biochemistry* **46**, 12979–12996 (2007).
28. A. J. Ninfa, P. Jiang, PII signal transduction proteins: Sensors of α-ketoglutarate that regulate nitrogen metabolism. *Curr. Opin. Microbiol.* **8**, 168–173 (2005).
29. C. Y. Huang, J. E. Ferrell Jr., Ultrasensitivity in the mitogen-activated protein kinase cascade. *Proc. Natl. Acad. Sci. U.S.A.* **93**, 10078–10083 (1996).
30. Y. Kim, M. Coppey, R. Grossman, L. Ajuria, G. Jiménez, Z. Paroush, S. Y. Shvartsman, MAPK substrate competition integrates pattern signals in the *Drosophila* embryo. *Curr. Biol.* **20**, 446–451 (2010).
31. Y. Kim, Z. Paroush, K. Nairz, E. Hafen, G. Jiménez, S. Y. Shvartsman, Substrate-dependent control of MAPK phosphorylation in vivo. *Mol. Syst. Biol.* **7**, 467 (2011).
32. P. Jiang, J. A. Peliska, A. J. Ninfa, Reconstitution of the signal-transduction bicyclic cascade responsible for the regulation of Ntr gene transcription in *Escherichia coli*. *Biochemistry* **37**, 12795–12801 (1998).
33. C. Gomez-Uribe, G. C. Verghese, L. A. Mirny, Operating regimes of signaling cycles: Statics, dynamics, and noise filtering. *PLoS Comput. Biol.* **3**, e246 (2007).
34. S. Jayanthi, D. Del Vecchio, Retroactivity attenuation in bio-molecular systems based on timescale separation. *IEEE Trans. Aut. Control* **56**, 748–761 (2010).
35. M. Behar, H. G. Dohlman, T. C. Elston, Kinetic insulation as an effective mechanism for achieving pathway specificity in intracellular signaling networks. *Proc. Natl. Acad. Sci. U.S.A.* **104**, 16146–16151 (2007).
36. J. Zhu, J. W. Burgner, E. Harms, B. R. Belitsky, J. L. Smith, A new arrangement of $(\beta/\alpha)_8$ barrels in the synthase subunit of PLP synthase. *J. Biol. Chem.* **280**, 27914–27923 (2005).

37. **Acknowledgments:** We thank A. Smith of the Janet Smith Laboratory (Life Sciences Institute, University of Michigan) for suggesting the use of the PLPS from the thermophile *G. stearothermophilus*, providing us with the expression plasmids for this enzyme, and suggesting purification methods. We thank S. Jayanthi for proofreading the paper. **Funding:** D.D.V. was supported in part by Air Force Office of Sponsored Research grant FA9550-10-1-0242. E.D.S. was partially supported by NIH grants 1R01GM086881 and 1R01GM100473-01. A.C.V. and S.D.M. were supported by grants from the Department of Defense Breast Cancer Research Program and the Center for Computational Medicine and Bioinformatics, University of Michigan. A.C.V. is a member of the Carrera del Investigador Científico (Consejo Nacional de Investigaciones Científicas y Técnicas). P.J. and A.J.N. were supported in part by GM059637. **Author contributions:** P.J., A.C.V., S.D.M., A.J.N., and D.D.V. designed the research; P.J. performed the experiments; D.D.V. and A.C.V. performed theoretical analysis; E.D.S., S.D.M., A.J.N., and D.D.V. analyzed the results; and A.J.N., A.C.V., E.D.S., and D.D.V. wrote the paper. **Competing interests:** The authors declare that they have no competing interests. **Data availability:** All experimental data are available upon request from A.J.N., and all simulation data are available upon request from D.D.V. The model file is available as part of the Supplementary Materials.

Submitted 2 May 2011
Accepted 19 September 2011
Final Publication 11 October 2011
10.1126/scisignal.2002152
Citation: P. Jiang, A. C. Ventura, E. D. Sontag, S. D. Merajver, A. J. Ninfa, D. Del Vecchio, Load-induced modulation of signal transduction networks. *Sci. Signal.* **4**, ra67 (2011).

Science Signaling
AAAS

www.sciencesignaling.org/cgi/content/full/4/194/ra67/DC1

Supplementary Materials for

Load-Induced Modulation of Signal Transduction Networks

Peng Jiang, Alejandra C. Ventura, Eduardo D. Sontag, Sofia D. Merajver, Alexander J. Ninfa,* Domitilla Del Vecchio*

*To whom correspondence should be addressed. E-mail: aninfa@umich.edu (A.J.N.); ddv@mit.edu (D.D.V.)

Published 11 October 2011, *Sci. Signal.* **4**, ra67 (2011)
DOI: 10.1126/scisignal.2002152

This PDF file includes:

Other Supplementary Material for this manuscript includes the following:
(available at www.sciencesignaling.org/cgi/content/full/4/194/ra67/DC1)

SimulinkModel (.mdl file)

1 Model and Simulation

We consider the covalent modification cycle with its targets as shown in Figure 1 A. Here, we analyze how the targets control the system transient response to the input stimulus u. We consider the standard two-step reaction model for enzymatic reactions [5]. Let E_1 and E_2 be the converter enzymes that convert protein W to its active form W* and protein W* back to the inactive form W, respectively. Let C_1 denote the complex of E_1 with W and C_2 be the complex of E_2 with W*. The reactions describing the system are given by

$$W + E_1 \underset{d_1}{\overset{a_1}{\rightleftharpoons}} C_1 \xrightarrow{k_1} W^* + E_1$$

$$W^* + E_2 \underset{d_2}{\overset{a_2}{\rightleftharpoons}} C_2 \xrightarrow{k_2} W + E_2.$$

Both the inactive and active protein forms bind to targets L and N, respectively, to form complexes $\bar{C}$ and C, respectively. In Figure 1 A, λ and α denote "effective" loads resulting from the binding to targets and are given by the amounts of targets normalized by their dissociation constants as explained in what follows. We add the binding reaction of W with its targets L $W + L \underset{k_{off}}{\overset{k_{on}}{\rightleftharpoons}} C$, and the binding of W* with its targets N $W^* + N \underset{\bar{k}_{off}}{\overset{\bar{k}_{on}}{\rightleftharpoons}} \bar{C}$.

The rate equations governing the system are given by

$$\begin{aligned}
\frac{dW}{dt} &= -a_1 W E_1 + d_1 C_1 + k_2 C_2 - k_{on} L W + k_{off} C \\
\frac{dC_1}{dt} &= a_1 W E_1 - (d_1 + k_1) C_1 \\
\frac{dW^*}{dt} &= -a_2 W^* E_2 + d_2 C_2 + k_1 C_1 - \bar{k}_{on} N W^* + \bar{k}_{off} \bar{C} \\
\frac{dC_2}{dt} &= a_2 W^* E_2 - (d_2 + k_2) C_2 \\
\frac{dC}{dt} &= k_{on} L W - k_{off} C \\
\frac{d\bar{C}}{dt} &= \bar{k}_{on} N W^* - \bar{k}_{off} \bar{C}.
\end{aligned}$$

To this differential equations, we add the algebraic equations expressing the conservation laws for the protein and the enzymes:

$$W_T = W + W^* + C_1 + C_2 + C + \bar{C},\ E_{1T} = E_1 + C_1,\ E_{2T} = E_2 + C_2.$$

Assuming $k_{off}, k_{on}, \bar{k}_{on}, \bar{k}_{off}, a_1, a_2, d_1, d_2 \gg k_1, k_2$ and $W_T \gg E_{1T}, E_{2T}$, we can employ the quasi steady state approximation (QSSA). Hence, we have that $\frac{dC_1}{dt} = 0$, $\frac{dC_2}{dt} = 0$, $\frac{dC}{dt} = 0$, and $\frac{d\bar{C}}{dt} = 0$. From these, we obtain that

$$C_1 = \frac{E_{1T} W}{K_1 + W} \text{ with } K_1 = (d_1 + k_1)/a_1, \quad C_2 = \frac{E_{2T} W^*}{K_2 + W^*} \text{ with } K_2 = (d_2 + k_2)/a_2$$

and that

$$C = L/k_D,\ \bar{C} = N/\bar{k}_D, \text{ with } k_D = k_{off}/k_{on},\ \bar{k}_D = \bar{k}_{off}/\bar{k}_{on}.$$

Since $\bar{W} = W^* + \bar{C} =$, we have that $\frac{d\bar{W}}{dt} = \frac{dW^*}{dt} + \frac{d\bar{C}}{dt} = -a_2 W^* E_2 + d_2 C_2 + k_1 C_1$, so that

$$\frac{d\bar{W}}{dt} = -a_2 W^* \frac{K_2 E_{2T}}{K_2 + W^*} + d_2 W^* \frac{E_{2T}}{K_2 + W^*} + k_1 \frac{E_{1T} W}{K_1 + W}.$$

Letting $\lambda := \frac{L}{k_D}$, $\alpha := \frac{N}{k_D}$, considering that $a_2 K_2 = d_2 + k_2$, $W^* = \bar{W}/(1+\alpha)$, and $W = (W_T - \bar{W})/(1+\lambda)$, we finally obtain

$$\frac{d\bar{W}}{dt} = V_1 \frac{W_T - \bar{W}}{K_1(\lambda+1) + (W_T - \bar{W})} - V_2 \frac{\bar{W}}{K_2(1+\alpha) + \bar{W}}, \tag{1}$$

in which $V_1 = k_1 E_{1T}$ and $V_2 = k_2 E_{2T}$ are the speeds of modification. Note that in the case in which $\alpha = 0$, we have that $\bar{C} = 0$ and we obtain as a special case of our derivations the situation in which the load is applied only to W.

This is the same differential equation as obtained in [2], in which the Michaelis-Menten constants are multiplied by a factor that increases with the amounts of downstream load. When $\lambda = \alpha = 0$, we obtain the differential equation for the system without the downstream load. Note that the differential equation for the free active protein concentration W^* would differ. Here, we focus on the total active protein dynamics because it is what can be measured in our experimental system.

Furthermore, if we assume that the activity of the enzymes are regulated by an allosteric effector u, which acts, for example, as an absolute activator for E_2 and as a non-competitive inhibitor for E_1, we obtain the following ordinary differential equation (ODE) model:

$$\frac{d\bar{W}}{dt} = \frac{V_1}{(1 + u/k'_D)} \frac{W_T - \bar{W}}{K_1(1+\lambda) + (W_T - \bar{W})} - V_2 \left(\frac{u}{\bar{k}'_D + u} \right) \frac{\bar{W}}{K_2(1+\alpha) + \bar{W}}, \tag{2}$$

in which k'_D and $\bar{k}'_D$ are the dissociation constants for the binding of u with E_1 and E_2, respectively. This model is also the same as the one of [2], in which the Michaelis-Menten constants are multiplied by factors that depend on the load. In this model, the (time-varying) input stimulus is given by $u(t)$. The results that we will obtain regarding the effects of the load on the dynamic response of $\bar{W}(t)$ to $u(t)$ are independent on whether there is an allosteric effector that regulates the activity of the enzymes. Specifically, similar results can be obtained for model (1) in which the input stimulus is given by $V_2(t)$ or by $V_1(t)$. Since in the experimental system, the input stimulus is an allosteric effector, we will carry the detailed analysis for this case.

1.1 Effects of the load on the steady state input/output response: stoichiometric retroactivity

In order to understand the effect of the load on the dynamic response of the system, we first recall the effect of sequestering by downstream targets on the steady states of an upstream system, that is, stoichiometric retroactivity [7] . Solving the ODE model (2) for the equilibrium by setting $\frac{d\bar{W}}{dt} = 0$, we obtain that $\bar{W}$ satisfies the equation

$$S = \frac{(W_T - \bar{W})(K_2(1+\alpha) + \bar{W})}{\bar{W}(K_1(1+\lambda) + W_T - \bar{W})}, \tag{3}$$

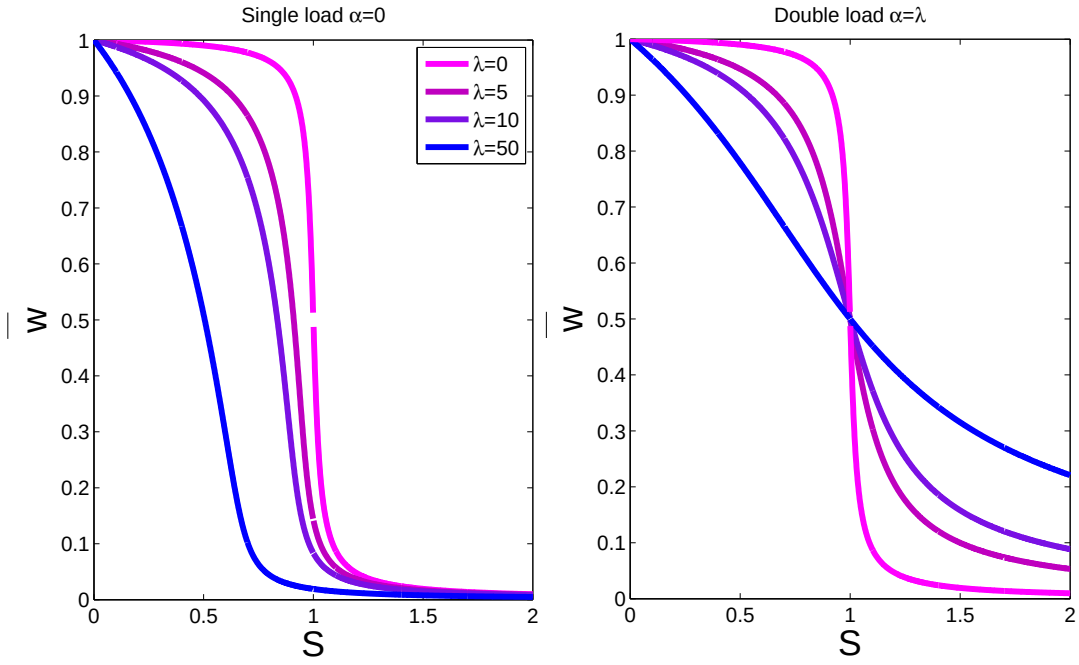

Figure S 1: **Steady state effects of loading.** Left: Effect of L_T on the steady state response of $\bar{W}$ to u when the load is applied only to W, that is, $N = 0$ so that $\alpha = 0$. Right: Effect of the load N on the steady state response of $\bar{W}$ to u when the load is applied to both W and W^*, and L=N, $k_D = \bar{k}_D = 1$, $K_1 = K_2 = 0.01$ and $W_T = 1$.

in which $S = V_2 \left(\frac{u}{k'_D+u}\right) / \left(\frac{V_1}{(1+u/k'_D)}\right)$. We plot in Figure S 1 the steady state values of $\bar{W}$ for varying amounts of S (the reader is referred to [7] for more details). In the case in which the load is applied on both W and W^*, the curves with different values of load cross all at the same point. This can be shown as follows. Assuming that L=N, that is, the downstream target is the same for both W and W*, which is the case in the experimental system, we have that $\alpha = \lambda \frac{\bar{k}'_D}{\bar{k}_D}$. Hence, we can re-write equation (3) as

$$S(\lambda, \bar{W}) = \frac{(W_T - \bar{W})(K_2(1 + \lambda \frac{\bar{k}'_D}{\bar{k}_D}) + \bar{W})}{\bar{W}(K_1(1+\lambda) + W_T - \bar{W})}.$$

For the family of curves in the (S, λ) plane to cross all at the same point for different values of λ, we have to request that there is a value $\bar{W}_0$, not dependent on α, such that $\frac{\partial S}{\partial \lambda}(\lambda, \bar{W}_0) = 0$. This gives:

$$\bar{W}_0 = \frac{K_2(\frac{\bar{k}'_D}{\bar{k}_D} K_1 + \frac{\bar{k}'_D}{\bar{k}_D} W_T - K_1)}{K_2 \frac{\bar{k}'_D}{\bar{k}_D} + K_1},$$

which is acceptable if and only if

$$\frac{\bar{k}'_D}{\bar{k}_D} K_1 + \frac{\bar{k}'_D}{\bar{k}_D} W_T - K_1 > 0 \text{ and } K_2 K_1 \frac{\bar{k}'_D}{\bar{k}_D} - K_2 K_2 - W_T K_1 < 0.$$

If this condition on the parameters is satisfied, then all steady state characteristics cross at the same point for varying amounts of load.

The qualitative effect of increasing the load, when applied to both sides, is to make the steady state response of the system linear for larger input variations about the crossing point. When the load is applied to one side only, that is, $\alpha = 0$, the major effect of the load is on the decrease of the value of the S_{50}, that is, the value of S corresponding to half-maximal response.

1.2 Characteristics of the dynamic response

In order to characterize the effect of the load on the dynamic response of the system, that is, load-induced modulation, we quantify the rise time, the decay time, the bandwidth and amplitude of response as functions of the load. Specifically, we define these quantities as follows. Let W_0 be the initial state of the cycle, that is, $W(0) = W_0$ and let W_{eq} be the steady state value corresponding to a constant input stimulus u.

Decay time. If $W_0 > W_{eq}$, we define the decay time as

$$t_{decay} = t_{10} - t_{90},$$

in which

$$t_{10} = \{t \mid \bar{W}(t) = W_0 + 0.9(W_{eq} - W_0)\}, \text{ and } t_{90} = \{t \mid \bar{W}(t) = W_0 + 0.1(W_{eq} - W_0)\}.$$

Rise time. if $W_0 < W_{eq}$, we define the rise time as

$$t_{rise} = t_{90} - t_{10},$$

in which

$$t_{90} = \{t \mid \bar{W}(t) = W_0 + 0.9(W_{eq} - W_0)\}, \text{ and } t_{10} = \{t \mid \bar{W}(t) = W_0 + 0.1(W_{eq} - W_0)\}.$$

Basically, the rise time quantifies the time $\bar{W}$ takes to rise from 10% of its overall excursion $|W_{eq} - W_0|$ to 90% of it, while the decay time quantifies the time $\bar{W}$ takes to decay from 90% of its overall excursion $|W_{eq} - W_0|$ to 10% of it. Other definitions of rise and decay times consider excursions of the signal between 5% and 95% or between 1% and 99%. The results of this paper do not depend on these specific values.

Bandwidth. Consider a periodic input stimulus $u(t)$ with period T. Let $\omega := \frac{2\pi}{T}$ be the frequency of the input stimulus and $A(\omega)$ be the amplitude of the permanent response of $\bar{W}(t)$ corresponding to input frequency ω. Note that it can be formally shown that the permanent response exists for the reduced system in equation (2) (see [6], for example). Let $A(0)$ be the amplitude of response when $\omega \to 0$. Then, the bandwidth of the system, denoted ω_B, is defined as the frequency at which the amplitude drops below $1/\sqrt{2}A(0)$, that is, ω_B is such that

$$A(\omega_B) = \frac{A(0)}{\sqrt{2}}.$$

The bandwidth of a system indicates how frequently a time-varying input stimulus can change before the system becomes incapable of responding to it. The bandwidth is usually calculated by applying small amplitude sinusoidal input stimuli at different frequencies and by measuring the

corresponding amplitude of response. Even though sinusoidal input stimuli are not necessarily biologically relevant, the system response to these inputs provides information on the amplitude of response and bandwidth even for more complicated input profiles. We therefore base our analysis on these types of inputs. However, since input profiles that have the shape of train of pulses are most often found in practice and in particular in our experiments, we complement our analysis on sinusoidal input stimuli with an analysis that considers the effect of both the period and the shape of the pulse profile on the system response.

1.3 Load-induced modulation of rise and decay times

We first consider the times the cycle takes to switch between "off" (fully unmodified) and "on" (fully modified) states in response to extreme inputs u, that is, $u = 0$ or $u \approx \infty$. When the inputs are extreme, the modification rates in equation (2) do not depend on the input u anymore as the modification speeds saturate to their extreme values. In this case, we say that the cycle operates in the zero-order regime. We then turn our attention to consider the transition time between states corresponding to intermediate values of the input u for which the modification speeds are not saturated. In this case, we say that the cycle operates in the first-order regime.

1.3.1 Transition times between "on" and "off" states

For the decay time, we have that the final steady state is $W_{eq} = 0$ corresponding to $u = \infty$ and the initial steady state value is $W_0 = W_T$ corresponding to $u = 0$. For the rise time, we have that the final steady state is $W_{eq} = W_T$ corresponding to $u = 0$ and the initial steady state is $W_0 = 0$ corresponding to $u = \infty$.

Decay time. For sufficiently large input stimuli u, we have that $\frac{V_1}{(1+u/k'_D)} \approx 0$ and that $\frac{u}{k'_D+u} \approx 1$, so that equation (2) reduces to

$$\frac{d\bar{W}}{dt} = -V_2 \frac{\bar{W}}{K_2(1+\alpha)+\bar{W}},\ \bar{W}(0) = W_T. \tag{4}$$

This differential equation can be directly integrated through the method of separation of variables as follows. Re-write it as

$$\frac{K_2(1+\alpha)+\bar{W}}{\bar{W}} d\bar{W} = -V_2 dt,$$

which, integrating the left-hand side between $\bar{W} = \bar{W}(0)$ and $\bar{W} = \bar{W}(t)$ and the right-hand side between $t = 0$ and t yields

$$\int_{\bar{W}(0)}^{\bar{W}(t)} \left(\frac{K_2(1+\alpha)}{\bar{W}} + 1 \right) d\bar{W} = -V_2 t,$$

which yields to

$$K_2(1+\alpha)(\ln(\bar{W}(t)) - \ln(\bar{W}(0))) + \bar{W}(t) - \bar{W}(0) = -V_2 t.$$

This, in turn yields to

$$t = \frac{1}{V_2} \left(K_2(1+\alpha) \ln \left(\frac{W_T}{\bar{W}(t)} \right) + W_T - \bar{W}(t) \right). \tag{5}$$

From this expression, we can approximate t_{10} and t_{90} by

$$t_{10} = \frac{1}{V_2}\left(K_2(1+\alpha)\ln(10) + 0.9W_T\right) \text{ and } t_{90} = \frac{1}{V_2}\left(K_2(1+\alpha)\ln(1.1) + 0.1W_T\right),$$

so that

$$t_{decay} = \frac{1}{V_2}\left(K_2(1+\alpha)\ln(10/1.1) + 0.8W_T\right). \tag{6}$$

Therefore, since $\alpha > 0$, the system with load applied to W^* displays an increased decay time compared to the system with no load applied to W^*. Furthermore, the decay time increases with the total amount of protein W_T and with the Michaelis-Menten constant K_2 of the reverse covalent modification reaction, while increasing the amount of enzyme E_2 decreases the decay time. Also, note that the decay time only depends on the parameters of the reverse covalent modification reaction.

Rise time. For sufficiently small input stimuli, we have that $\frac{V_1}{(1+u/k'_D)} \approx V_1$ and that $\frac{u}{k'_D+u} \approx 0$, so that equation (2) reduces to

$$\frac{d\bar{W}}{dt} = V_1\frac{W_T - \bar{W}}{K_1(1+\lambda) + (W_T - \bar{W})},\ \bar{W}(0) = 0. \tag{7}$$

This differential equation can be directly integrated using the method of separation of variables as follows. Let $w := W_T - \bar{W}$, then the above ODE in the new variable w becomes

$$\frac{dw}{dt} = -V_1\frac{w}{K_1(1+\lambda) + w},\ w(0) = W_T,$$

which yields to

$$K_1(1+\lambda)\frac{w(t)}{w(0)} + w(t) - w(0) = -V_2 t,$$

in which, substituting $w(t) = W_T - \bar{W}(t)$ and $w(0) = W_T$ finally gives

$$K_1(1+\lambda)\frac{W_T}{W_T - \bar{W}(t)} + \bar{W}(t) = V_2 t.$$

This, in turn yields to

$$t = \frac{1}{V_1}\left(K_1(1+\lambda)\ln\left(\frac{W_T}{W_T - \bar{W}(t)}\right) + \bar{W}(t)\right) \tag{8}$$

From this expression, we can approximate t_{10} and t_{90} by

$$t_{10} = \frac{1}{V_1}\left(K_1(1+\lambda)\ln(1.1) + 0.1W_T\right) \text{ and } t_{90} = \frac{1}{V_1}\left(K_1(1+\lambda)\ln(10) + 0.9W_T\right),$$

so that

$$t_{rise} = \frac{1}{V_1}\left(K_1(1+\lambda)\ln(10/1.1) + 0.8W_T\right). \tag{9}$$

Therefore, since $\lambda > 0$, the system with load applied to W displays an increased rise time compared to the system with no load applied to W. Furthermore, the rise time increases with

the total amount of protein W_T and with the Michaelis-Menten constant K_1 of the forward covalent modification reaction, while increasing the amount of enzyme E_1 decreases the rise time. Also, note that the rise time only depends on the parameters of the forward covalent modification reaction. The results are summarized in Figure 2 A.

Remark. A similar result on the rise and decay times can be obtained for more general dynamic equations using the comparison theorem for scalar ordinary differential equation [1]. Specifically, consider the scalar equation

$$\dot{x} = f_\lambda(x,u) - g_\alpha(x,u),$$

in which we assume that $f \equiv 0$ when $u = \infty$ and that $g \equiv 0$ when $u = 0$. Furthermore, we assume that if $\lambda_1 < \lambda_2$ and $\alpha_1 < \alpha_2$ then $f_{\lambda_1}(x,u) > f_{\lambda_2}(x,u)$ and $g_{\alpha_1}(x,u) > g_{\alpha_2}(x,u)$. Without loss of generality, we assume that $\dot{x} = f_\lambda(x,u)$ has $x = 1$ as global attractor and that $\dot{x} = -g_\alpha(x,u)$ has $x = 0$ as global attractor. Hence, if we start from initial condition $x(0) < 0.1$ and $u = 0$, we have that the solution of $\dot{x} = f_0(x,u)$ will always be larger for any t than the solution of $\dot{x} = f_\lambda(x,u)$ for all $\lambda > 0$. As a consequence, the rise time will be smaller when $\lambda = 0$, that is, for the unloaded system. Similarly, if we start from initial condition $x(0) = 0.9$ and $u = \infty$, we have that the solution of $\dot{x} = -g_0(x,u)$ will always be smaller for any t than the solution of $\dot{x} = -g_\alpha(x,u)$ for all $\alpha > 0$. As a consequence, the decay time will be smaller when $\alpha = 0$, that is, for the unloaded system.

Remark. Note that if one had taken the definition of rise and decay times based on different percentages from 10% and 90%, say x% and y%, one would have obtained for the decay and rise times:

$$t_{decay} = \frac{1}{V_2}\left(K_2(1+\alpha)\ln(x/y) + (0.0y - 0.0x)W_T\right)$$

and

$$t_{rise} = \frac{1}{V_1}\left(K_1(1+\lambda)\ln((1-0.0x)/(1-0.0y)) + (0.0y - 0.0x)W_T\right),$$

which have the same behavior as expressions (6),(9).

1.3.2 Transition times between intermediate states

We next investigate the relationship between the rise and decay times for the isolated and connected systems when the input stimulus u is set to some intermediate value. For this sake, define

$$v_1 := \frac{V_1}{(1+u/k'_D)} \text{ and } v_2 := V_2\left(\frac{u}{\bar{k}'_D + u}\right),$$

which represent the maximal speeds of the forward and reverse modification reactions, respectively, for a given value of the allosteric effector concentration u. Here, we seek to show that when the isolated system is ultrasensitive, that is, $K_1, K_2 \ll W_T$, if W_0 and W_{eq} are not too small nor too close to W_T, we have that the connected system rise and decay times become smaller than those of the isolated system when $v_1 - v_2 \to 0$ for sufficiently high load. Specifically, as the value of u is changed to make the maximal modification speeds approach each other, then (for sufficiently large loads) we have that the isolated system transient response becomes slower than the connected system transient response. We make this precise by mathematically stating our assumptions as follows.

Assumptions. The isolated system is ultrasensitive, that is, $K_1, K_2 \ll W_T$, and the initial condition W_0 and equilibrium value W_{eq} of $\bar{W}$ satisfy $(W_T - W_0), (W_T - W_{eq}) \gg K_1$ and $W_0, W_{eq} \gg K_2$. Furthermore, we assume that the load is large enough so that $\bar{K}_1 \gg W_T$ and $\bar{K}_2 \gg W_T$.

Claim 1. *Under the above stated assumptions, for $(v_1 - v_2)$ sufficiently small we have that $t^C_{rise} < t^I_{rise}$ and $t^C_{decay} < t^I_{decay}$, in which "I" stands for "Isolated" and "C" Stands for "Connected".*

Proof. Isolated system. Under the above stated assumptions, we have that $K_1 \ll (W_T - \bar{W}(t))$ and $K_2 \ll \bar{W}(t)$ so that, we can approximate system (2) by

$$\frac{d\bar{W}}{dt} \approx v_1 - v_2 \text{ for } 0 < \bar{W}(t) < W_T,$$

and $\frac{d\bar{W}}{dt} = 0$ otherwise, in which $v_1 > v_2$ for u sufficiently small and $v_1 < v_2$ for u sufficiently large. This equation can be integrated to obtain that $\bar{W}(t) = W_0 + (v_1 - v_2)t$, which holds while $\bar{W}(t) < W_{eq}$ for $(v_1 - v_2) > 0$ and while $\bar{W}(t) > W_{eq}$ for $(v_1 - v_2) < 0$. The rise and decay times can be computed employing the definition, which leads to

$$t^I_{rise} = 0.8\frac{W_{eq} - W_0}{v_1 - v_2} \text{ and } t^I_{decay} = 0.8\frac{W_0 - W_{eq}}{v_2 - v_1}.$$

If one had used different percentages in the definition of rise and decay times, the above expression would stay the same except for having a different coefficient in place of 0.8. Note that when $(v_1 - v_2) \to 0$, we have that $W_{eq} \to \frac{W_T K_2}{K_1 + K_2}$, which is a value that does not depend on $(v_1 - v_2)$. Hence, as $(v_1 - v_2) \to 0$, we have that $t_{rise}, t_{decay} \to \infty$, that is, the response becomes arbitrarily slow as v_1 and v_2 approach each other.

Connected system. Here, we consider two cases: $\alpha > 0$ (double load) and $\alpha = 0$ (single load). When $\alpha > 0$, we have that $\bar{K}_1, \bar{K}_2 \gg W_T$ by the assumption, so that we can approximate system (2) by

$$\frac{d\bar{W}}{dt} = \frac{W_T v_1}{\bar{K}_1} - \bar{W}\left(\frac{v_1}{\bar{K}_1} + \frac{v_2}{\bar{K}_2}\right).$$

If instead $\alpha = 0$, we can approximate it by

$$\frac{d\bar{W}}{dt} = \frac{v_1 W_T}{\bar{K}_1} - v_2 - \bar{W}\left(\frac{v_1}{\bar{K}_1}\right).$$

Letting $\delta := \frac{v_1}{\bar{K}_1} + \frac{v_2}{\bar{K}_2}$ when $\alpha > 0$ and $\delta := \frac{v_1}{\bar{K}_1}$ when $\alpha = 0$, the rise and decay times are both equal to

$$t^C_{rise} = t^C_{decay} = \frac{\ln(9)}{\delta}.$$

As a consequence, for a fixed load, there is a sufficiently small value of $v_1 - v_2$ such that $t^C_{rise}, t^C_{decay} < t^I_{rise}, t^I_{decay}$. If one had used different percentages in the definition of rise and decay times, the above expression would stay the same except for having a different coefficient in place of $\ln(9)$.

□

Hence, we can conclude that when the input stimulus u is such that v_1 and v_2 are very close to each other and the isolated system has an ultrasensitive response, then when the load is high enough to move the system to the hyperbolic regime, the connected system response to constant input stimuli is faster than that of the isolated system. Figure 2 B shows how the isolated system response is slower when v_1 and v_2 are closer to each other and how the connected system becomes faster than the isolated system in such a case.

Remark. Note that if $K_1, K_2 \gg W_T$, which implies that the steady state response is hyperbolic, then the loaded system will always be slower even for intermediate values of the input stimulus.

As a final remark on rise and decay times, note that different values of the Michaelis-Menten constants K_1 and K_2 can lead to qualitatively different effects of the load on the rise and decay times for intermediate values of the input stimulation. This point is shown in Figure 2 C. This fact can be explained as follows. Assume first that $V_1 = V_2$. When $v_1/v_2 \gg 1$ or $v_2/v_1 \gg 1$, having $K_1 < K_2$ ($K_2 < K_1$) implies that $t^I_{rise} < t^I_{decay}$ ($t^I_{rise} > t^I_{decay}$) from equations (6,9). Also, with the load, we have that $t^I_{rise} < t^C_{rise}$ and $t^I_{decay} < t^C_{decay}$ from the same equations. With a load α, λ such that $K_1(1+\lambda) \approx K_2(1+\alpha)$ we also have that $t^C_{rise} \approx t^C_{decay}$. When (v_1/v_2) becomes closer to 1, we have (by Claim 1) that t^I_{rise} and t^I_{decay} both increase. Hence, there is a value of (v_1/v_2) for which $t^I_{decay} > t^C_{decay}$ ($t^I_{decay} < t^C_{decay}$) but $t^I_{rise} < t^C_{rise}$ ($t^I_{rise} > t^C_{rise}$). In theory, by making (v_1/v_2) approach 1, also t^I_{rise} (t^I_{decay}) should become larger than t^C_{rise} (t^C_{decay}). In practice, however, there may be limitations to how close to each other v_1 and v_2 can be made. More generally, assume that when $v_1/v_2 \gg 1$ or $v_2/v_1 \gg 1$ we have that $t^I_{rise} < t^I_{decay}$ ($t^I_{rise} > t^I_{decay}$) and that the load is such that $t^C_{rise} \geq t^C_{decay}$. Then, as (v_1/v_2) approaches 1, we have that $t^I_{decay} > t^C_{decay}$ ($t^I_{decay} < t^C_{decay}$) but $t^I_{rise} < t^C_{rise}$ ($t^I_{rise} > t^C_{rise}$) unless (v_1/v_2) is made very close to 1, which is possible in theory but may be practically hard to realize.

1.4 Load-induced modulation of the frequency response

In this section, we study the effect of the load on the response to periodic input stimuli. Specifically, we consider the response to sinusoidal input stimuli both for the isolated and connected systems. In the next section, we consider more general input stimuli to validate the results obtained with sinusoidal inputs.

We consider periodic inputs of the form $u(t) = u_0 + A_0 \sin(\omega t)$, in which $u_0 > A_0$ is the mean value, or bias, A_0 is the amplitude of the signal about the mean, which is supposed to be small, and ω is the frequency, that is, $\omega = 2\pi/T$ in which T is the period of the signal. We compute the amplitude of the response, the bandwidth, and the effect on the amplitude of changes in the amounts of enzymes E_{1T} and E_{2T}. In what follows, we first consider the case in which the system is loaded on both sides, that is, $\alpha \neq 0$ and $\lambda \neq 0$. In this case, we can choose a value of u_0 such that the corresponding steady state values for the isolated and connected systems are the same for all values of load (see right-side plots of Figure S 1). This substantially simplifies the analysis. Let thus the bias term u_0 be such that $(u_0, \bar{W}_0)$ is a steady state for both the isolated and connected systems.

Assuming the amplitude A_0 to be sufficiently small, we can employ the linear approximation of system (2) about the equilibrium $(u_0, \bar{W}_0)$ [3,4]. Letting $\bar{K}_1 := K_1(1+\lambda)$ and $\bar{K}_2 := K_2(1+\alpha)$

to simplify notation, consider the ODE model for the system

$$\frac{d\bar{W}}{dt} = \frac{V_1}{(1+u/k'_D)}\frac{W_T-\bar{W}}{\bar{K}_1+(W_T-\bar{W})} - V_2\left(\frac{u}{\bar{k}'_D+u}\right)\frac{\bar{W}}{\bar{K}_2+\bar{W}},$$

and assume that A_0 is sufficiently small so that the change of $\bar{W}$ about $\bar{W}_0$, that is, $\Delta\bar{W} = \bar{W}-\bar{W}_0$ is small enough so that the dynamics of $\Delta\bar{W}$ are well approximated by the linearization of the above system about $(u_0, \bar{W}_0)$, that is,

$$\frac{d\Delta\bar{W}}{dt} = -\left(\frac{u_0V_2}{\bar{k}'_D+u_0}\frac{\bar{K}_2}{(\bar{K}_2+\bar{W}_0)^2} + \frac{k'_DV_1}{k'_D+u_0}\frac{\bar{K}_1}{(\bar{K}_1+(W_T-\bar{W}_0))^2}\right)\Delta\bar{W} -$$

$$\left(\frac{\bar{k}'_D}{(\bar{k}'_D+u_0)^2}\frac{\bar{W}_0V_2}{\bar{K}_2+\bar{W}_0} + \frac{k'_DV_1}{(k'_D+u_0)^2}\frac{W_T-\bar{W}_0}{\bar{K}_1+(W_T-\bar{W}_0)}\right)A_0\sin(\omega t).$$

Letting

$$\delta = \frac{u_0V_2}{\bar{k}'_D+u_0}\frac{\bar{K}_2}{(\bar{K}_2+\bar{W}_0)^2} + \frac{k'_DV_1}{k'_D+u_0}\frac{\bar{K}_1}{(\bar{K}_1+(W_T-\bar{W}_0))^2} \tag{10}$$

and

$$\beta = \frac{\bar{k}'_D}{(\bar{k}'_D+u_0)^2}\frac{\bar{W}_0V_2}{\bar{K}_2+\bar{W}_0} + \frac{k'_DV_1}{(k'_D+u_0)^2}\frac{W_T-\bar{W}_0}{\bar{K}_1+(W_T-\bar{W}_0)}. \tag{11}$$

this differential equation can be integrated to obtain

$$\Delta\bar{W}(t) = -\frac{A_0\beta}{\sqrt{\omega^2+\delta^2}}\sin(\omega t-\tan^{-1}(\omega/\delta)) - \frac{A_0\beta\omega}{\omega^2+\delta^2}e^{-\omega_B t},$$

from which we obtain the expression of the amplitude

$$A(\omega) = \frac{A_0\beta}{\sqrt{\omega^2+\delta^2}}. \tag{12}$$

We call δ the *cycle flux* and it quantifies the speed of the conversion reactions when the cycle operates in a small neighborhood of the equilibrium point $(u_0, \bar{W}_0)$. Note that it depends on the amount of load. Here, we explicitly consider two different cases based on whether the isolated system has an ultrasensitive response ($K_1, K_2 \ll W_T$) or whether it has a hyperbolic response (K_1, K_2 are comparable to W_T). In fact, the dependency of the cycle flux on the load is qualitatively different in these two cases and will result in different bandwidths.

Case 1 (Double load and ultrasensitive isolated system steady state response: $K_1, K_2 \ll W_T$). In this case, assuming also that $\bar{W}_0, W_T-\bar{W}_0 \gg K_1, K_2$, the expressions of β and δ are well approximated by β^I and δ^I, in which "I" stands for "Isolated", given by

$$\beta^I = \frac{V_1k'_D}{(k'_D+u_0)^2} + \frac{V_2\bar{k}'_D}{(\bar{k}'_D+u_0)^2}, \text{ and } \delta^I = 0.$$

As a consequence, the amplitude for the isolated system response $A^I(\omega)$ is well approximated by

$$A^I(\omega) = \begin{cases} \min\{\bar{W}_0, W_T-\bar{W}_0\} & \text{if } \omega \le \omega_B^I/\sqrt{2} \\ \frac{\beta^IA_0}{\omega} & \text{if } \omega > \omega_B^I/\sqrt{2}, \end{cases} \tag{13}$$

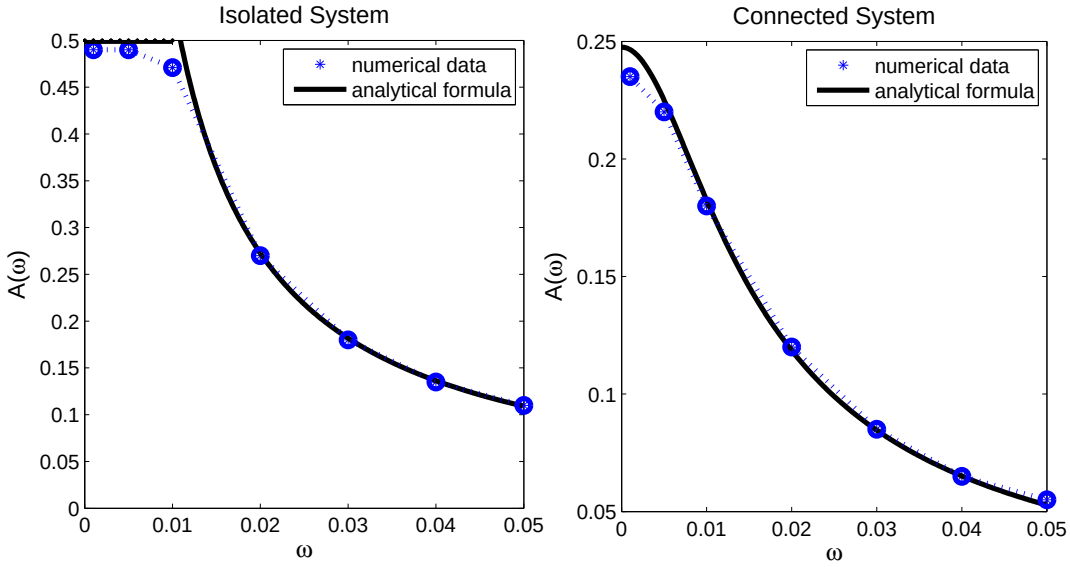

Figure S 2: **Effect of loading on the frequency response.** Numerical simulation data (dashed line) against the analytically predicted values of the amplitudes (solid line) for both the isolated (left) and connected (right) systems from the formulas in equations (13) and (14), respectively. Here, we have set $A_0 = 0.5, u_0 = 1$, $k'_D = \bar{k}'_D = 2$, $K_1 = K_2 = 0.01$, $V_2 = \bar{k}'_D V_1$, $V_1 = 0.01$, $\alpha = \lambda = 50$, $W_T = 1$.

in which

$$\omega_B^I = \frac{\sqrt{2}\beta^I A_0}{\min\{\bar{W}_0, W_T - \bar{W}_0\}}$$

is the bandwidth of the isolated system. For the connected system, if $\frac{A_0\beta^C}{\delta^C} \leq \min\{\bar{W}_0, W_T - \bar{W}_0\}$ then we have that

$$A^C(\omega) = \frac{A_0\beta^C}{\sqrt{\omega^2 + (\delta^C)^2}}, \text{ and } \omega_B^C = \delta^C \tag{14}$$

in which "C" denotes "Connected", and δ^C and β^C are given by the expressions of δ and β given in equations (10)-(11) evaluated at the non-zero load values α and λ. From theory, these expressions hold for A_0 small enough. Figure S 2 shows that in practice these expressions hold for quite large values of A_0. So, in this case, we have that the bandwidth of the connected system is smaller than that of the isolated system, that is, $\omega_B^C < \omega_B^I$ if $\delta^C < \frac{\sqrt{2}\beta^I A_0}{\min\{\bar{W}_0, W_T - \bar{W}_0\}}$, which is satisfied for large enough loads since $\delta^C \to 0$ as $(\lambda, \alpha) \to \infty$. If we have that $\frac{A_0\beta^C}{\delta^C} > \min\{\bar{W}_0, W_T - \bar{W}_0\}$, then the amplitude expression of equation (14) holds only for ω sufficiently large and the bandwidth is not equal to the cycle flux δ^C but to $\omega_B^C = \sqrt{\frac{2A_0^2(\beta^C)^2}{\min\{\bar{W}_0, W_T - \bar{W}_0\}^2} - (\delta^C)^2}$, which is always smaller than ω_B^I. Hence, we conclude that for large enough loads, the bandwidth of the connected system is smaller than that of the isolated system, that is, $\omega_B^C < \omega_B^I$.

Case 2 (Double load and hyperbolic isolated system steady state response: K_1, K_2 comparable with W_T). If $W_T - K_1 \leq \bar{W}_0 \leq K_2$, then the cycle flux δ is a monotonically decreasing function

of the load, therefore we have that $\delta^I > \delta^C$. If A_0 is small enough so that $\frac{A_0\beta^I}{\delta^I}, \frac{A_0\beta^C}{\delta^C} < \min\{\bar{W}_0, W_T - \bar{W}_0\}$, we have that $\omega_B^C = \delta^C$ and $\omega_B^I = \delta^I$ so that for all values of the load $\omega_B^C < \omega_B^I$, that is, the bandwidth of the connected system is always smaller than that of the isolated system.

Case 3 (Single load). We conclude by considering the effect of the load when it is applied only to W, that is, $\alpha = 0$ but $\lambda \neq 0$. In this situation, the equilibrium of the connected system is always lower than the equilibrium of the isolated system for all input values (Figure S 1) and the linear approximation of system (2) holds only for very small values of A_0. Hence, the conclusions of the analysis depend on the specific choice of the bias input u_0, which provides different steady state values $\bar{W}_0$ for the isolated and connected systems. Note that too large values of u_0 will result in an almost zero response of the loaded system (left side plot of Figure S 1). If u_0 is sufficiently small, $K_2 \ll \bar{W}_0$, and $(W_T - \bar{W}_0) < K_1$, the cycle flux can be well approximated by

$$\delta^C \approx \frac{k'_D}{k'_D + u_0} \frac{\bar{K}_1}{(\bar{K}_1 + (W_T - \bar{W}_0))^2},$$

which is a monotonically decreasing function of the load λ. Hence, we obtain that $\delta^C < \delta^I$ and that $\omega_B^C < \omega_B^I$, that is, the bandwidth of the connected system is smaller than the bandwidth of the isolated system. A more general analysis of the single load system considering large amplitude deviations from the equilibrium is dealt with in the next section.

Figure 3 summarizes the behavior of the bandwidth as a function of the load, the Michaelis-Menten constants, and the input amplitude.

1.4.1 Effects of the enzymes amounts

Case 1 (Double load and ultrasensitive isolated system steady state response: $K_1, K_2 \ll W_T$) We next study the effect of the enzyme amounts, specifically of V_1 and V_2, on the relative difference $\Delta = \frac{A^I(\omega) - A^C(\omega)}{A^I(\omega)}$ between the amplitudes of the isolated and connected systems. Letting for simplicity $V_2 = aV_1$ and $V_1 = V$, we have for sufficiently large frequency ω that $\Delta = 1 - \frac{\beta^C \omega}{\beta^I \sqrt{w^2 + (\delta^C)^2}}$, which decreases as V decreases (because $\frac{\beta^C \omega}{\beta^I \sqrt{w^2 + (\delta^C)^2}}$ increases as V decreases). Hence, as V decreases, that is, the amounts of enzymes decrease, the amplitudes of the connected and isolated system approach each other. This is also shown in Figure S 3. Finally, since the amplitude can never exceed $\min\{\bar{W}_0, W_T - \bar{W}_0\}$, we also have that $A^C(0) \leq A^I(0)$.

Case 2 (Double load and hyperbolic isolated system steady state response: K_1, K_2 comparable with W_T). Furthermore, letting for simplicity $V_2 = aV_1$ and $V_1 = V$, we have for sufficiently large frequency ω that $\Delta = 1 - \frac{\beta^C \sqrt{w^2 + (\delta^I)^2}}{\beta^I \sqrt{w^2 + (\delta^C)^2}}$, which, since $\delta^C < \delta^I$, is an increasing function of V (because $\frac{\beta^C \sqrt{w^2 + (\delta^I)^2}}{\beta^I \sqrt{w^2 + (\delta^C)^2}}$ is a decreasing function of V). As a consequence, when the value of V_1 decreases, that is, the amounts of enzymes decrease, the amplitudes of the connected and isolated systems become further apart from each other. This is opposite to the result obtained for Case 1. Furthermore, when $\omega \to 0$ the behavior of $\bar{W}(t)$ is practically at the quasi steady state and hence it exactly tracks the steady state characteristics of the right-side plot of Figure S 1. Hence, the amplitude of the response of the connected system is smaller than that of the isolated system, that is, $A^C(0) \leq A^I(0)$.

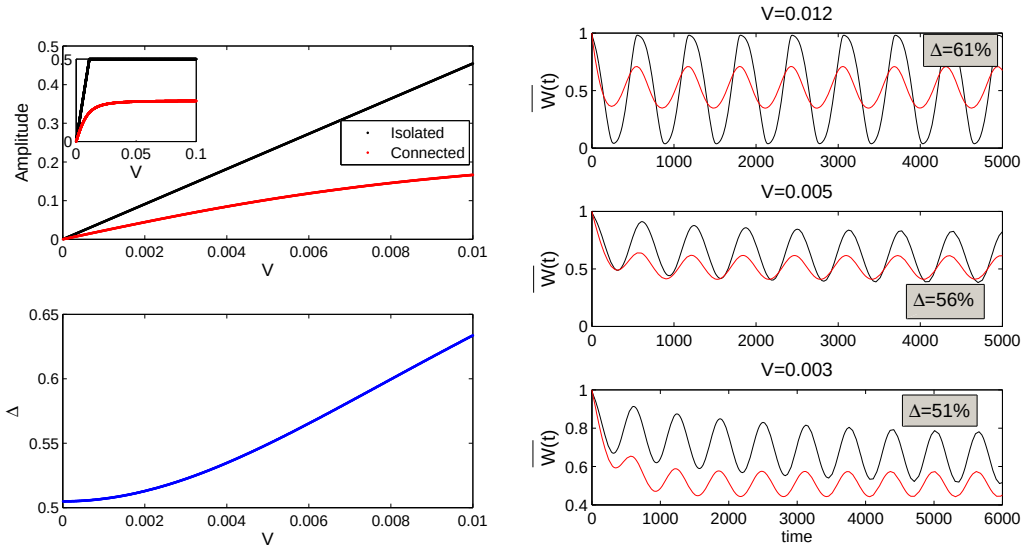

Figure S 3: **Effects of enzymes amounts.** In the left plots, we show the behavior of the amplitudes of the connected (red) and isolated (black) systems as function of V as obtained from the analytical expressions of Table 1. Here, Δ is the difference between the isolated and connected system amplitudes divided by the amplitude of the isolated system. It represents the percentage difference between the amplitudes in the two systems. In the right-side plots, we show data obtained through numerical simulation for three different values of V. As predicted from the analytical expressions, as V decreases, the percentage difference between the two amplitudes decreases. Here, we have set $A_0 = 0.5, u_0 = 1$, $k'_D = \bar{k}'_D = 2$, $K_1 = K_2 = 0.01$, $V_2 = \bar{k}'_D V_1$, $V_1 = V$, $\omega = 0.01$, $\alpha = \lambda = 50$, $W_T = 1$.

Case 3 (Single load). Since $\delta^C < \delta^I$, we have that $\Delta = 1 - \frac{\beta^C \sqrt{w^2+(\delta^I)^2}}{\beta^I \sqrt{w^2+(\delta^C)^2}}$ is an increasing function of V. Hence, as the amounts of enzymes decrease, the amplitudes of the connected and isolated systems become further apart from each other.

The results are summarized in Figure 3 D.

1.5 Input Stimuli as Trains of Pulses with Saturating Amplitudes

In the previous section, we have analyzed the response of the system to periodic (sinusoidal) input profiles of small amplitude of period $T = 2\pi/\omega$. In this section, we consider input stimuli in the form of pulses of large amplitude applied at periods of length T. We assume each pulse to have an exponential profile, that is, $u_M e^{-lt}$, in which u_M is the pulse height and $l > 0$ is the decay rate of the pulse. The input stimulus can be thus written as

$$u(t) = u_0 + u_M \sum_{k=0}^{\infty} e^{-l(t-kT)} 1(t - KT),$$

in which $1(t - kT) = 0$ if $t < kT$ and $1(t - kT) = 1$ otherwise. These types of inputs are more realistic than sinusoidal inputs and in particular are those found in the experiments that we performed. Although the general findings about the effects of targets on the amplitude

and bandwidth of the previous section carry to general types of inputs (as any input can be expressed as an infinite combination of sinusoidal functions), in this and the next section we seek to specifically determine the effect of both u_M and l on the amplitude of response to the pulse.

In this section, we assume that the pulse height u_M and the decay rates are comparably large enough ($u_M \gg k'_D, \bar{k}'_D$ and $l \gg 1$) so that that there are time intervals T_1 and T_2 with $T_1 + T_2 = T$ such that in any period of length T we have that $\frac{V_1}{(1+u/k'_D)} \approx 0$ and $\left(\frac{V_2 u}{k'_D+u}\right) \approx V_2$ for T_1 seconds, while $\frac{V_1}{(1+u/k'_D)} \approx V_1$ and $\left(\frac{u}{k'_D+u}\right) \approx 0$ for T_2 seconds. In such a case, the amplitude of the response can be calculated by directly integrating equation (2) under the assumptions that the steady state characteristics of the isolated system are in the ultrasensitive regime ($K_1, K_2 \ll W_T$) and that for the loaded system, the load is sufficiently large.

Let $t_0, t_0+T, t_0+2T, ..., t_0+kT$ be the sequence of times at which the input pulse is applied. Assuming the pulse height is very large, we approximate the dynamics of the system for every $k > 0$ by

$$\frac{d\bar{W}}{dt} = -V_2 \frac{\bar{W}}{K_2(1+\alpha) + \bar{W}}, \text{ for } t \in [t_0 + kT, t_0 + kT + T_1]$$

$$\frac{d\bar{W}}{dt} = V_1 \frac{W_T - \bar{W}}{K_1(\lambda+1) + (W_T - \bar{W})}, \text{ for } t \in [t_0 + kT + T_1, t_0 + kT + T_1 + T_2],$$

in which T_1 is the duration of time in which the approximation $\frac{V_2 u}{(k'_D+u)} \approx V_2$ and $\frac{V_1}{(1+u/k'_D)} \approx 0$ hold and $T_1 + T_2 = T$. Under this approximation, we can integrate the above differential equations to obtain (letting $\bar{K}_1 = K_1(1+\lambda)$ and $\bar{K}_2 = K_2(1+\alpha)$) the following algebraic equations for the lower peaks $\bar{W}(t_0 + kT + T_1)$ and for the upper peaks $\bar{W}(t_0 + kT)$, with $\bar{W}(t_0) = W_T$

$$\bar{K}_2 \ln\left(\frac{\bar{W}(t_0 + kT + T_1)}{\bar{W}(t_0 + kT)}\right) + \bar{W}(t_0 + kT + T_1) - \bar{W}(t_0 + kT) + V_2 T_1 = 0, \tag{15}$$

and

$$\bar{K}_1 \ln\left(\frac{W_T - \bar{W}(t_0 + kT + T_1)}{W_T - \bar{W}(t_0 + (k+1)T)}\right) + \bar{W}(t_0 + (k+1)T) - \bar{W}(t_0 + kT + T_1) - V_1 T_2 = 0, \tag{16}$$

respectively. Now, we study the isolated and connected system cases separately.

Isolated System. Since the isolated system is assumed to operate in the ultrasensitive regime, we have that $K_1, K_2 \ll W_T$. We can thus neglect in expressions (15-16) the terms multiplying K_1 and K_2 so that we obtain the sequences of the upper peaks as

$$\{W_T, W_T - V_2T_1 + V_1T_2, W_T - 2V_2T_1 + 2V_1T_2, ..., W_T - kV_2T_1 + kV_1T_2\}$$

and for the lower peaks as

$$\{W_T - V_2T_1, W_T - 2V_2T_1 + V_1T_2, W_T - 3V_2T_1 + 2V_1T_2, ..., W_T - (k+1)V_2T_1 + kV_1T_2\}.$$

So, by taking the difference between the upper peaks and lower peaks and considering that this difference cannot exceed W_T, we obtain the following expression for the difference between the

upper and lower peaks:

$$A = \begin{cases} V_1T_2 & \text{if } V_2T_1 \geq V_1T_2 \text{ and } W_T \geq V_1T_2 \\ W_T & \text{if } V_2T_1 > V_1T_2 \text{ and } W_T < V_1T_2 \\ \min\{W_T, V_2T_1\} & \text{if } V_2T_1 < V_1T_2 \text{ and } V_2T_1 > W_T \\ \min\{W_T, V_2T_1\} & \text{if } V_2T_1 < V_1T_2 \text{ and } V_2T_1 < W_T, \end{cases}$$

from which, merging the second to last case, we obtain that

$$A = \begin{cases} V_1T_2 & \text{if } V_2T_1 \geq V_1T_2 \text{ and } W_T \geq V_1T_2 \\ \min\{W_T, V_2T_1\} & \text{if } V_2T_1 < V_1T_2 \text{ or } V_2T_1 > V_1T_2 > W_T, \end{cases}$$

which, simplifying the conditions of the cases, finally leads to

$$A = \begin{cases} V_1T_2 & \text{if } V_1T_2 \leq \min\{W_T, V_2T_1\} \\ \min\{W_T, V_2T_1\} & \text{if } V_1T_2 > \min\{W_T, V_2T_1\}, \end{cases}$$

from which, substituting $T_2 = 2\pi/\omega - T_1$, we obtain the final expression for the amplitude as

$$A^I(\omega) = \begin{cases} \min\{V_2T_1, W_T\} & \text{if } \omega \leq \frac{2\pi V_1}{T_1V_1 + \min\{T_1V_2, W_T\}} \\ \frac{2\pi V_1}{\omega} - V_1T_1 & \text{if } \omega > \frac{2\pi V_1}{T_1V_1 + \min\{T_1V_2, W_T\}}, \end{cases} \tag{17}$$

in which the bandwidth ω_B^I is given by

$$\omega_B^I = \frac{2\sqrt{2}\pi V_1}{T_1V_1 + \sqrt{2}\min\{T_1V_2, W_T\}}.$$

Expression (17) is a good approximation, especially at low frequencies as seen in Figure S 4 and hence it is a suitable means for calculating the bandwidth of the isolated system. The analytical expression of the amplitude reaches zero for the value of ω such that $T_2 = 0$ because in such a case the effective input to the system also has zero amplitude.

Connected System (double load). For the connected system, assuming the load is sufficiently large, the values of $\bar{K}_1$ and $\bar{K}_2$ are large enough so that in expressions (15-16) we can neglect the linear terms. This way, denoting by $\lambda_1 = V_2T_1/\bar{K}_2$ and by $\lambda_2 = V_1T_2/\bar{K}_1$, we obtain the sequence of upper peak values as

$$\{W_T, W_T(1 - e^{-\lambda_2} + e^{-(\lambda_1+\lambda_2)}), W_T(1 - e^{-\lambda_2} + e^{-(\lambda_1+\lambda_2)} - e^{-(\lambda_1+2\lambda_2)} + e^{-(2\lambda_1+2\lambda_2)}), ...\}.$$

In particular, one can calculate the limit of this sequence by using the limit of a geometric series and obtain that the upper peaks tend to

$$W_T\left(1 - \frac{(1 - e^{-\lambda_1})e^{-\lambda_2}}{1 - e^{-\lambda_2-\lambda_1}}\right).$$

Similarly, the sequence of lower peaks is given by

$$\{W_Te^{-\lambda_1}, W_T(e^{-\lambda_1} - e^{-(\lambda_1+\lambda_2)} + e^{-(2\lambda_1+\lambda_2)}), ...\},$$

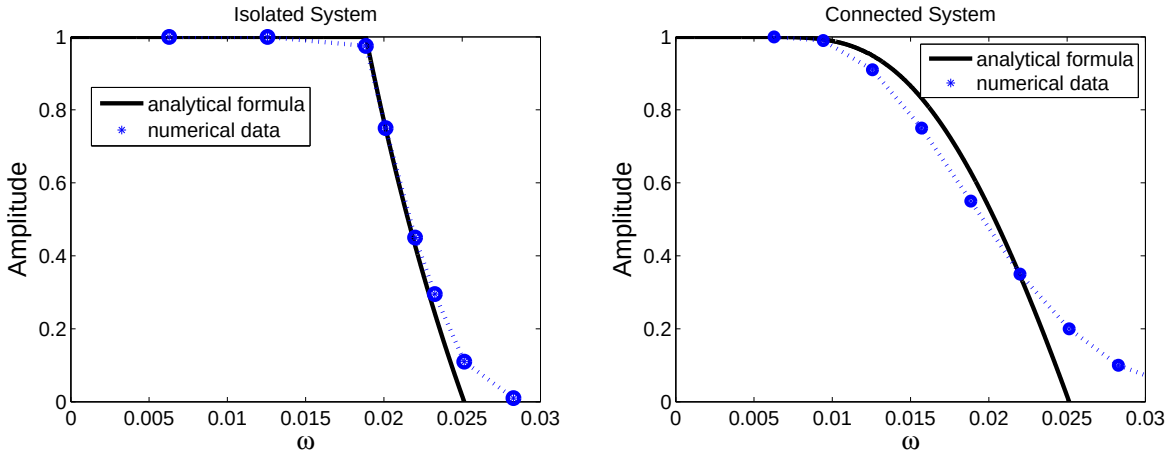

Figure S 4: **Effect of the load on the amplitude of response to a train of pulses.** the left plots, we show the behavior of the amplitude of the isolated system of equation (17) (solid) compared to numerical simulation data (dashed) obtained for $u(t)$ equal to a train of pulses of width equal to $T_1 = 250$. In the right-side plots we show the behavior of the amplitude of the connected system of equation (18) (solid) compared to numerical simulation data (dashed). Here, we have set $k'_D = \bar{k}'_D = 2$, $K_1 = K_2 = 0.01$, $V2 = \bar{k}'_D V_1$, $V_1 = V = 0.012$, $\alpha = \lambda = 100$, $W_T = 1$.

which is also a monotonically decreasing sequence. Its limit can be computed by using again the limit of a geometric series to obtain

$$W_T \left(1 - \frac{1 - e^{-\lambda_1}}{1 - e^{-\lambda_2 - \lambda_1}}\right).$$

By computing the difference between the limit of the lower peaks and the limit of the upper peaks and letting $\lambda_1 = V_2 T_1 / \bar{K}_2$ and $\lambda_2 = V_1 T_2 / \bar{K}_1$, we obtain

$$A^C(\omega) = W_T \frac{(1 - e^{-\lambda_1})(1 - e^{-V_1/\bar{K}_1(2\pi/\omega - T_1)})}{1 - e^{-\lambda_1 - V_1/\bar{K}_1(2\pi/\omega - T_1)}}, \tag{18}$$

which is a good approximation for sufficiently large values of T_2, that is, for sufficiently low frequencies (right-side plot of Figure S 4). Hence, it is a suitable expression for calculating the bandwidth of the system. For values of T_2 approaching zero, the analytical expression of the amplitude approaches zero because $\frac{V_1}{(1+u/k'_D)} \approx 0$ and $\left(\frac{u}{k'_D + u}\right) \approx V_2$ for all t and thus also the stimulation has effectively zero amplitude. The expression (18) can be employed to calculate the bandwidth of the system as

$$\omega_B^C = \frac{2\pi V_1}{V_1 T_1 + \bar{K}_1 \ln\left(\frac{\sqrt{2} - e^{-\lambda_1}}{\sqrt{2} - 1}\right)},$$

which becomes smaller as T_1 and/or the load increases. In particular, as λ increases, this bandwidth monotonically decreases, but as α increases also, the decrease of this bandwidth is not as dramatic. Hence, when the load applied to W is much larger than the load applied to W*, the decrease of bandwidth due to the load is more dramatic. In particular, the above

expression holds when the load on both W and W* is large enough. In this case, we have that $\bar{K}_1 \ln\left(\frac{\sqrt{2}-e^{-\lambda_1}}{\sqrt{2}-1}\right) \approx \frac{K_1(1+\lambda)}{K_2(1+\alpha)}\frac{V_2T_1}{\sqrt{2}-1}$. Hence, the value of ω_B^C is smaller than that of ω_B^I as long as $\frac{K_1(1+\lambda)}{K_2(1+\alpha)} > \sqrt{2}-1$.

By contrast, if the load is applied to W only, that is, $\alpha = 0$, we obtain the following approximated expressions for the amplitude and bandwidth, respectively (see the Appendix for the derivations):

$$A^C(\omega) = \begin{cases} V_2T_1 & \text{if } \omega \le \omega_B^C \\ W_T(1-\exp\left(-\frac{V_1}{K_1}(\frac{2\pi}{\omega}-T_1)\right) & \text{if } \omega > \omega_B^C, \end{cases} \tag{19}$$

in which

$$\omega_C^B = \frac{2\pi V_1}{V_1T_1 + \bar{K}_1 \ln\left(\frac{1}{1-V_2T_1/W_T}\right)}. \tag{20}$$

Connected system (single load: $\alpha = 0$). In this case, we have that $\bar{K}_1 = K_1$ and assuming still that the system operates in the ultrasensitive regime ($K_1, K_2 \ll W_T$), we obtain the amplitude as

$$A^C(\omega) = \begin{cases} V_2T_1 & \text{if } \omega \le \frac{2\pi V_1}{V_1T_1+\bar{K}_1\ln\left(\frac{1}{1-V_2T_1/W_T}\right)} \\ W_T(1-\exp(-\frac{V_1(2\pi/\omega-T_1)}{\bar{K}_1})) & \text{if } \omega > \frac{2\pi V_1}{V_1T_1+\bar{K}_1\ln\left(\frac{1}{1-V_2T_1/W_T}\right)}, \end{cases} \tag{21}$$

from which the bandwidth is computed as

$$\omega_B^C = \frac{2\pi V_1}{V_1T_1 + \bar{K}_1 \ln\left(\frac{1}{1-V_2T_1/(\sqrt{2}W_T)}\right)}. \tag{22}$$

This bandwidth monotonically decreases with the load λ.

Summary. When the load is applied to both W and W*, if K_1 and K_2 are the same, and the load is equally distributed between W and W*, then the bandwidth of the connected system is lower than that of the isolated system. In general, when the effective Michaelis-Menten constant of the forward reaction in the loaded system, that is, $K_1(1+\lambda)$, is larger than the effective Michaelis-Menten constant of the backward reaction, that is, $K_2(1+\alpha)$, then the loaded system will display a smaller bandwidth. In Figure S 4, for example, the bandwidth of the loaded system is much smaller than that of the isolated system. When the load is applied to W only, the bandwidth is a monotonically decreasing function of the load λ. Comparing expression (22) to expression (20), it follows that if $\alpha \approx \lambda$, the bandwidth decreases more dramatically in the system with single load than in the system with double load when the load λ increases.

We finally examine the trend of the upper and lower peaks of the responses as well as the bias level of the response when both α and λ are nonzero.

Peaks. The values of the upper and lower peaks for both the isolated and connected systems monotonically decrease and approach each other for high enough values of the frequency of the input stimulation. Therefore, for high enough values of the frequency, the response of both the connected and isolated systems will tend to constant values, which are the smallest values each of the systems (isolated and connected) can reach.

Bias level. The value of the enzyme amounts, that is, the value of V influences the relative location of the bias values of the signals subject to periodic input stimuli. Specifically, the location of the lower peaks of the isolated system when $V_1T_2 > V_2T_1$ is given by $W_T - V_2T_1$. By contrast, the lower peaks of the connected system are at $W_T(1 - \frac{1-e^{-\lambda_1}}{1-e^{-\lambda_1-\lambda_2}})$, in which $\lambda_1 = V_2T_1/\bar{K}_2$ and $\lambda_2 = V_1T_2/\bar{K}_1$. If $V_2 = aV_1$ and $V_1 = V$ with V very small, this expression is well approximated by $W_T\left(\frac{T_2/\bar{K}_1}{aT_1/\bar{K}_2+T_2/\bar{K}_1}\right)$. For V small enough, we thus have that $W_T - aVT_1 > W_T\left(\frac{T_2/\bar{K}_1}{aT_1/\bar{K}_2+T_2/\bar{K}_1}\right)$, which implies that the bias of the connected system response will be smaller than the bias of the isolated system response.

The bias level is also affected by the frequency ω. Specifically, when ω increases we have that T_2 becomes very small and approaches zero. When T_2 approaches zero, we have that $-V_2\left(\frac{u}{k'_D+u}\right) \approx -V_2$ while $\frac{V_1}{(1+u/k'_D)} \approx 0$ for all time. If there is a basal level V_0 for the forward reaction, the dynamics of both the connected and isolated systems are given by

$$\frac{d\bar{W}}{dt} = -V_2\frac{\bar{W}}{\bar{K}_2 + \bar{W}} + V_0.$$

Starting from $\bar{W}(0) = W_T$, the system reaches the steady state $\bar{W} = \frac{V_0}{V_1-V_0}\bar{K}_2$. Since $\bar{K}_2 = K_2(1+\alpha)$ and $\alpha = 0$ for the system without the load, then the final steady state reached for the isolated system is higher than the final steady state reached by the connected system.

2 Experimental Systems

In this section, we describe in more detail the development of the experimental system for measurement of responses to time-varying input stimulation by the reconstituted UTase/UR-PII cycle and provide additional data on the response time.

In addition to the two experiments that were averaged in Figure 4 E, we examined the decay time in experiments where glutamine was added to 0.5 mM, 0.8 mM, and 1.5 mM, all of which are non-saturating levels of stimulation. Hence, the cycle operates in the first-order regime. Conditions for these experiments are in the legend for Figure S 5. As shown in Figure S 5, when glutamine was added to 0.5 mM, we could not detect a difference in decay time between isolated and connected systems. When glutamine was injected to 0.8 mM, the isolated system appeared to be slower than did the isolated system. When glutamine was injected to 1.5 mM, the connected system again appeared to be faster than the isolated system, but only marginally so (Figure S 5). Thus, targets could speed up the response to stimulation with intermediate glutamine concentrations, but only within a narrow range of the intermediate glutamine concentrations.

The rise time of the system was also observed under conditions of intermediate stimulation, using both wild-type and heterotrimeric PII and at a variety of glutamine concentrations. These experiments were conducted using the same conditions described for measuring rise-time in the main text, except that intermediate concentrations of glutamine were present. As shown in Table 2, under no conditions did we identify a glutamine concentration at which the rise time of the connected system was faster than was the rise time of the isolated system. The general trend was that the difference between isolated and connected system became smaller as the glutamine concentration was increased (Table 1). Thus, in our experimental system targets

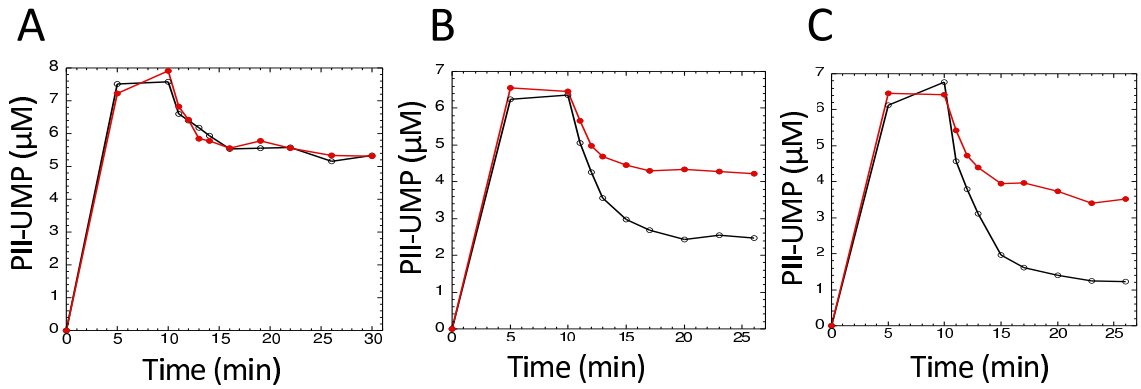

Figure S 5: **Response of the UTase/UR-PII cycle to stimulation with nonsaturating concentrations of glutamine.** Reaction conditions were 100 mM Tris-Cl, pH 7.5, 100 mM KCl, 10 mM MgCl, 0.3 mg/mL bovine serum albumin, 3 μM PII, 1.5 μM UTase/UR, 0.2 mM α-ketoglutarate, 1 mM UTP, 1 mM ATP, and NRII at 0 (black curves and points) or 10 μM (red curves and points). Reactions were incubated in the absence of glutamine for 10 min, after which glutamine was added. A. Glutamine was added to 0.5 mM. B. Glutamine was added to 0.8 mM. C. Glutamine was added to 1.5 mM. Note that panel B is a different experiment than the two experiments used to produce Figure 4 E in the main text, and thus serves as an additional repeat of that experiment.

had an asymmetrical effect upon intermediate stimulation (at 0.8 mM glutamine), it made responses faster in one direction while making responses in the opposite direction slower.

To impose a relaxation oscillator-type time-varying input signal, we included an enzyme that consumes glutamine in the reaction mixtures, and periodically injected glutamine into the system. Suitable glutaminase enzymes were not available commercially, as we required an enzyme with a low K_m to efficiently remove low concentrations of glutamine from our systems, and the enzyme must have sufficient catalytic rate to efficiently operate in the time frame of our *in vitro* experiments. A useful glutaminase proved to be the pyridoxal phosphate synthase from the thermophile *Geobacillus stearothermophilus*; we used this enzyme in the absence of its other targets, ribose-5-phosphate and glyceraldehyde-3-phosphate because additional studies showed that these, curiously, decreased the rate of glutamine consumption. The pyridoxal phosphate synthase (PLPS) consists of two types of subunits (S and T) forming a 24-mer, in which the T subunits catalyze glutamine conversion to glutamate, but only when in the 24-mer. In some experiments, we added additional T subunits to ensure that the 24-mer was saturated with this subunit. Figure S 6 shows how this glutaminase can be used to create time-varying input signals. In the two experiments shown, uridylylation of PII was allowed to occur in the absence of glutamine, resulting in complete modification of PII, and glutamine was injected when shown by the arrow. In Figure S 6A, the reaction mixtures contained different levels of glutaminase, and a low concentration of glutamine was injected (2.5 mM). When no glutaminase was present, PII uridylylation state fell to the low level characteristic of 2.5 mM glutamine, and stayed there (bottom curve). As glutaminase was increased, increasingly shallow dips in the level of PII uridylylation were observed. That is, as the rate of decay of the input signal (glutamine) was increased, the amplitude of response decreased as expected from our theoretical analysis. In Figure S 6B, a saturating glutamine concentration was injected (5

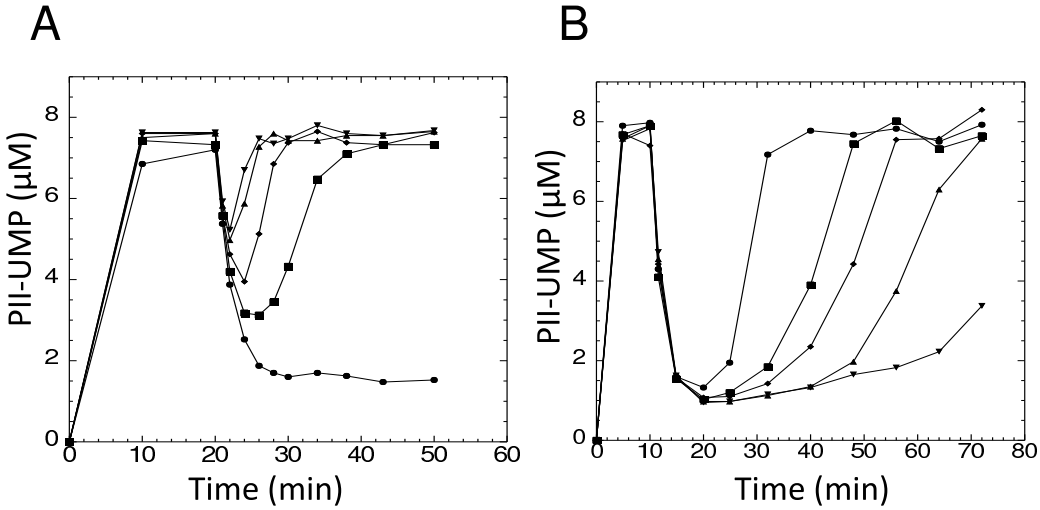

Figure S 6: **Using glutaminase and injections of glutamine to impose time-varying input stimulation**. A. Amplitude and time-course of the response to glutamine injection depend upon the concentration of glutaminase and attendant rate of glutamine decay. The UTase/UR-PII monocycle was incubated in the absence of glutamine for 20 min and with different amounts of glutaminase present, allowing PII to become fully modified, after which glutamine was added to 2.5 mM (indicated by arrow). After the addition of glutamine, the amplitude of the response and the time it took for PII to become uridylylated again depended upon the amount of glutaminase that was present. Reaction conditions were: 100 mM Tris-Cl, pH 7.5, 100 mM KCl, 10 mM MgCl, 0.3 mg/mL bovine serum albumin, 3 μM PII, 1.5 μM UTase/UR, 0.2 mM α-ketoglutarate, 1 mM UTP, 1 mM ATP, and pyridoxyl phosphate synthase (all PLPS amounts stated include additional PdxT subunits in ratio PLPS 1: "extra" PdxT 0.2 to ensure saturation of enzyme with the PdxT subunit). The PLPS concentrations were (from lowest to highest curve) 0 μM, 50 μM, 100 μM, 150 μM, and 200 μM. B. At saturating stimulation, the time-course of the response depends upon the concentration of glutaminase present. Reaction mixtures were as above except lacking glutaminase, and were incubated in the absence of glutamine, allowing PII to become fully modified. After 10 min, glutamine was added to 5 mM, and simultaneously different concentrations of glutaminase were added. The glutaminase in this case consisted of purified PLPS 24-mer without addition of extra PdxT subunits. The time required for restoration of PII-UMP depended upon the concentration of glutaminase added; these concentrations were (fastest curves to slowest) 100 μM, 60 μM, 50 μM, 40 μM, and 30 μM.

mM), along with different levels of the glutaminase protein. In this case, the time required for the system to recover from the glutamine addition depended upon the level of glutaminase. In both experiments, the level of PII uridylylation eventually returned to the level obtained in the absence of glutamine, signifying that the K_m of the glutaminase is sufficiently low as to allow removal of glutamine from the reaction mixtures.

Measurement of the amplitudes of responses after glutamine addition proved to be dependent upon whether or not the system had attained a steady state prior to the first addition of glutamine. This issue is illustrated in Figure S 7. When the system had attained a steady state prior to the first addition of glutamine, the amplitude of the initial response was similar to

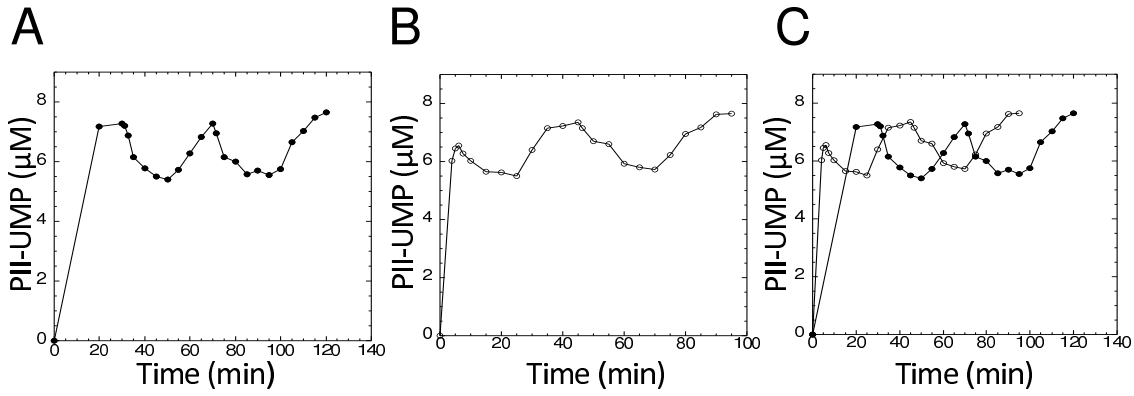

Figure S 7: **Amplitude of the initial response to glutamine addition depends on whether or not the system has achieved a steady state before glutamine addition.** Identical reaction conditions were used for the experiments shown in panels A and B, and panel C shows an overlay of these results. Reaction conditions were: 100 mM Tris-Cl, pH 7.5, 100 mM KCl, 10 mM MgCl, 0.3 mg/mL bovine serum albumin, 3 μM PII, 0.1 μM UTase/UR, 0.2 mM α-ketoglutarate, 1 mM UTP, 1 mM ATP, 10 μM NRII, 75 μM PLPS, and additional 15 μM pdxT subunit of PLPS. For panel A, the reaction mixture was incubated for 30 min in the absence of glutamine, after which glutamine was added to 5 mM at 30 min and again at 70 min. In this experiment, the system had achieved the steady state prior to the first addition of glutamine. For panel B, the reaction mixture was incubated for 5 min in the absence of glutamine, after which glutamine was added to 5 mM. A second injection of glutamine to 5 mM occurred at 45 min. In this experiment, the system had not yet attained the steady state at the 5 min point when the first addition of glutamine occurred. As shown in panel C, the amplitudes of the second response were similar, but the amplitudes of the first response were not, suggesting that amplitudes for the first response are strongly affected by whether the system had achieved the steady state.

that of a later injection of glutamine. However, a smaller amplitude of the initial response to glutamine was observed if the system had not yet attained the steady state prior to challenge with glutamine, while a later challenge in the same experiment yielded a response with higher amplitude (Figure S 7). Thus, the amplitude of the first response is unreliable, unless it is certain that the steady state had been attained before addition of glutamine. Because of this, we routinely ignored the first decay upon addition of glutamine, and measured amplitudes starting with the first rise in PII-UMP after glutamine addition.

References

[1] L. B. Bushard. Comparison theorems for scalar and vector second order nonlinear ordinary differential equations and inequalities. *Journal of Mathematical Analysis and Applications*, 52:561–572, 1975.

[2] A. Goldbeter and D. E. Koshland. An amplified sensitivity arising from covalent modification in biological systems. *Proc. Natl. Acad. Sci. USA*, pages 6840–6844, 1981.

[3] C. Gomez-Uribe, G. C. Verghese, and L. A. Mirny. Operating regimes of signaling cycles: Statics, dynamics, and noise filtering. *PLOS Computational Biology*, 3(12):2487–2497, 2007.

[4] H. Khalil. *Nonlinear Systems*. Prentice Hall, 2002.

[5] E. Klipp, R. Herwig, A. Kowald, C. Wierling, and H. Lehrach. *Systems Biology in Practice*. Wiley, 2005.

[6] G. Russo, M. di Bernardo, and E. D. Sontag. Global entrainment of transcriptional systems to periodic inputs. *Plos Computational Biology*, 2010.

[7] A. C. Ventura, P. Jiang, L. Van Wassenhove, D. Del Vecchio, S. D. Merajver, and A. J. Ninfa. Signaling properties of a covalent modification cycle are altered by a downstream target. *Proc. Natl. Acad. Sci. USA*, 107(22):10032–10037, 2010.